






RESEARCH ARTICLE

Among Land Snail Shells and Ashes: Geoarchaeological Analysis of the Maximiano Rockshelter, Southeast Brazil

Nicolás Batalla¹  | Mercedes Okumura²  | Casimiro S. Munita³  | Charles French⁴  | Astolfo G. M. Araujo⁵ 

¹Museum of Archaeology and Ethnology - MAE/USP, University of São Paulo, São Paulo, Brazil | ²Institute of Biosciences, University of São Paulo, São Paulo, Brazil | ³Nuclear and Energy Research Institute, IPEN-CNEN/SP, São Paulo, Brazil | ⁴McBurney Laboratory for Geoarchaeology, Department of Archaeology, University of Cambridge, Cambridge, UK | ⁵Museum of Archaeology and Ethnology, University of São Paulo—MAE/USP, São Paulo, Brazil

Correspondence: Nicolás Batalla (arnico.batalla@usp.br)

Received: 27 October 2024 | **Revised:** 14 December 2024 | **Accepted:** 14 January 2025

Scientific Editor: Sarah Sherwood

Funding: This research came from the São Paulo Research Foundation (FAPESP), under grants no. 2023/18132-2, 2018/14293-3, 2020/04283-0, 2013/13794-5, 2019/18664-9, and 2018/23282-5; the National Council for Scientific and Technological Development (CNPq) (Productivity in Research Fellowship 308856/2022-8), and the PRINT USP CAPES Exchange Visitor Program PVEJS 16/2020 (88887.569895/2020-00).

Keywords: atlantic forest | facies and microfacies | neotropics | rock-shelter settings | shell-matrix sites | site formation processes

ABSTRACT

Geoarchaeological studies, particularly those incorporating micromorphology and associated techniques, have revealed the complex depositional and post-depositional history of mollusk shell-matrix archaeological sites, mostly in coastal areas where these sites are more widespread. But geoarchaeology can also be crucial to disentangle human and natural agencies in inland shell-rich settings, including caves and rock-shelters. In this paper, the site formation processes of the land snail-rich Maximiano Rockshelter, located in the karstic upper Ribeira de Iguape River valley of southern São Paulo state, Southeast of Brazil, are tackled. Embedded in the neotropical Atlantic Forest, the site contains lithics, bone artifacts, and faunal and human remains dating between ~11,165 and 1282 cal year B.P. Facies and microfacies were characterized in exposed stratigraphic profiles through micromorphology, particle size analysis, major, minor, and trace elements, and FTIR spectroscopy. Despite the strong humification affecting most of the site, results indicate deposits resulting from anthropic activities such as the dumping of land snail shells and other remains, the tossing of entire and fragmented shells in sub-horizontally distributed layers, primary combustion features, and dumping/sweeping of combustion-derived materials. Shell-bearing facies exhibit similarities with chronologically contemporaneous Ribeira de Iguape basin's riverine *sambaquis*.

1 | Introduction

Multi-technique geoarchaeology offers a fundamental framework for unraveling mollusk shell-matrix sites by tackling, at different scales of observation, the complex array of depositional and post-depositional processes involved in their formation (Hale et al. 2021; Stein 1992a, 1992b; Stein et al. 2011; Szabó 2017; Thompson et al. 2016; Villagran 2019). Specifically, the characterization of human activities like dumping and tossing of shells and occupation-derived materials that constitute these sites, at times over millennia,

has been made possible by applying archaeological micromorphology coupled with several other techniques (Aldeias and Bicho 2016; Balbo et al. 2010; Beresford-Jones et al. 2022; Duarte et al. 2019; Grono et al. 2022; Power et al. 2022; Simões and Aldeias 2022; Villagran 2014, 2019; Villagran et al. 2021; Ward et al. 2019; Wurz et al. 2022).

As different categories of shell-matrix sites (from small middens to decametric mounds) are commonly encountered in coastal areas across the planet, geoarchaeological research has tended to focus on

Charles French is a Professor Emeritus

these contexts. But these sites also occur away from the coasts, alongside rivers and lakes (e.g., Claassen 2010; Figuti and Plens 2014; Furquim et al. 2021; Lombardo et al. 2013; Lubell 2004; Lubell et al. 1976; Moore and Thompson 2012; Pugliese et al. 2019; Rabett et al. 2011; Rick 2023; Zhang et al. 2024).

Some inland shell-rich sites share two characteristics: (1) they are embedded in rock-shelters and caves and (2) their main malacological component consists of land snails (e.g., Lloveras et al. 2011; Lubell 2004; Rabett et al. 2011; Taylor and Bell 2017). Unlike their counterparts with shells derived from aquatic mollusks, the anthropic origin of land snail shell deposits in sheltered settings is sometimes debated. Land snail life cycles, which can involve hibernation/estivation and carbonate supply for shell building, as well as their occasional transport by water, mass wasting, and animals like rodents and birds are cited as reasons behind this caution (Bonizzoni et al. 2009; Girod 2011; Hunt and Hill 2017). These issues are usually approached from archaeomalacological/zooarchaeological perspectives (e.g., Bernáldez-Sánchez and García-Iñás 2014; Hunt and Hill 2017; Lloveras et al. 2011; Taylor et al. 2011). However, just as in open-air contexts, geoarchaeology can play a crucial role in addressing the natural and cultural agencies behind shell-rich deposits in caves and rock-shelter settings (Goldberg 2000; Linstädter and Kehl 2012; McAdams et al. 2022; Morrissey et al. 2023; Simões et al. 2024; Wurz et al. 2022).

This has particular relevance in humid tropical areas, where sheltered environments present much higher preservation potential for perishable materials and anthropogenic deposits than open-air contexts (Araújo and Piló 2017; Friesem et al. 2016, 2017; Morley and Goldberg 2017; Silva et al. 2021).

In this paper, a multi-technique macro- and microstratigraphically based geoarchaeological approach is developed to assess the integrity, formation history, and preservation of anthropogenic materials and deposits at the Maximiano Rockshelter, a gastropod shell-rich site located in the Ribeira de Iguape River Basin, within the neotropical Atlantic Forest biome of southeastern Brazil. By combining archaeological micromorphology with multi-element and molecular analyses, this work aims at characterizing the human activities and natural agencies that are behind the site's deposits and transformations and establishing its insertion within the wider occupation of shell-matrix sites in this region.

1.1 | The Ribeira de Iguape River Valley and Its Archaeological Setting

Extending for ~80 km, the Ribeira de Iguape River valley constitutes one of few transitional regions between the mountain ranges bordering the continental plateaus and the Atlantic coastal plains in Brazil (Barreto 1988). Its main river, the Ribeira de Iguape, cuts across a lithologically diverse mountainous landscape and meanders through hilly lowlands before reaching the ocean at the Cananéia-Iguape estuarine complex in São Paulo State (Figure 1a–c) (Moss and Moss 2007). The valley contains the best preserved tract of tropical Atlantic forest, accounting for ~21% of Brazil's remaining 12.4% (Campanili and Schaffer 2010; Fundação SOS Mata Atlântica 2023).

Part of the upper and middle Ribeira de Iguape basin constitutes a speleological province integrated by the Açungui Group lithologies (Auler 2019). These comprise a sequence of metasedimentary rocks of Meso- to Neoproterozoic age encompassing both metasiliciclastic and metacarbonate formations crosscut by intrusive igneous bodies (Campanha and Sadowski 1999; Faleiros et al. 2012). The succession defines a landscape of mountain ridges and hills interconnected by karstic plateaus between 500 and 800 masl (Karmann and Ferrari 2002; Lenhare and Sallun Filho 2014). These features are more striking in the Upper Ribeira Tourist State Park (PETAR), a ~35.89 ha-wide conservation area on the left margin of the Ribeira de Iguape River (Ivanauskas et al. 2012) (see Figure 1c).

The presence of archaeological material in cave entrances and other speleological features in the area first attracted the attention of amateur and, later, professional archaeologists since the late XIXth century (Afonso 2019; Barreto et al. 1984; Chahud et al. 2023; Collet 1978a, 1978b, 1985, 2001; DeBlasis 1988, 1996, 1999; Felizardo 2017; Krone 1909; Parellada 2006; Robrahn 1988; Zenero 2022). This interest has often gone hand in hand with a focus on the most conspicuous evidence for a regional pre-European human presence, that is, the riverine *sambaquis*. These comprise shell-matrix sites (*sambaqui* means “shell heap” in Tupian indigenous languages) with a mean round or elliptical plan area of ~1000 m² and a height of up to 2 m, mostly located adjacent to rivers and streams (Barreto 1988; DeBlasis et al. 1994; Figuti et al. 2013; Sakai 1981) (see Figure 1c). Shells of the giant South American pulmonate terrestrial snail *Megalobulimus* spp. (see Bequaert 1948; Fontenelle and Miranda 2017) are the main malacological material of these sites, followed by those of the freshwater bivalve *Diplodon* spp. (Figuti and Plens 2014; Plens 2009; Penin 2005; Tognoli 2016). Both rock-shelter and riverine *sambaquis* have yielded the earliest hunter-gatherer occupations for the region, whose oldest dates stretch back to ~9810 year B.P. (11,165 median cal year B.P.; see Section 2 for radiocarbon calibration procedures) and ~9250 year B.P. (10,375 median cal year B.P.), respectively (Collet 1985; Ferraz et al. 2023; Figuti et al. 2013; Neves et al. 2005).

While the presence of gastropod shell-rich layers in cave entrances and rock-shelters had been known for some time (Krone 1909), it was the French speleologist and amateur archaeologist Guy-Christian Collet (1985) who championed the idea that they were part of the same archaeological expression as the riverine *sambaquis*. During the 1970s, Collet and collaborators (Collet 1978a, 1978b, 1985; Collet and Prous 1977; Collet and Guimarães 1977) carried out surveys and test-pit excavations within the basin. Within the context of that work, the Maximiano Rockshelter was discovered in the Iporanga county, ~92 km away from the Atlantic coast (see Figure 1c).

1.2 | The Maximiano Rockshelter

The archaeological site, facing southwest, sits at the base of a ~30-m-tall metacarbonate rock cliff (Figure 2a,b), which is part of the Caboclos/Casa de Pedra karstic area within PETAR park (Fundação Florestal 2018, p. 187–188) (see Figure 1c). The rock-shelter is tens of meters away from the resurgence of the Maximiano river from

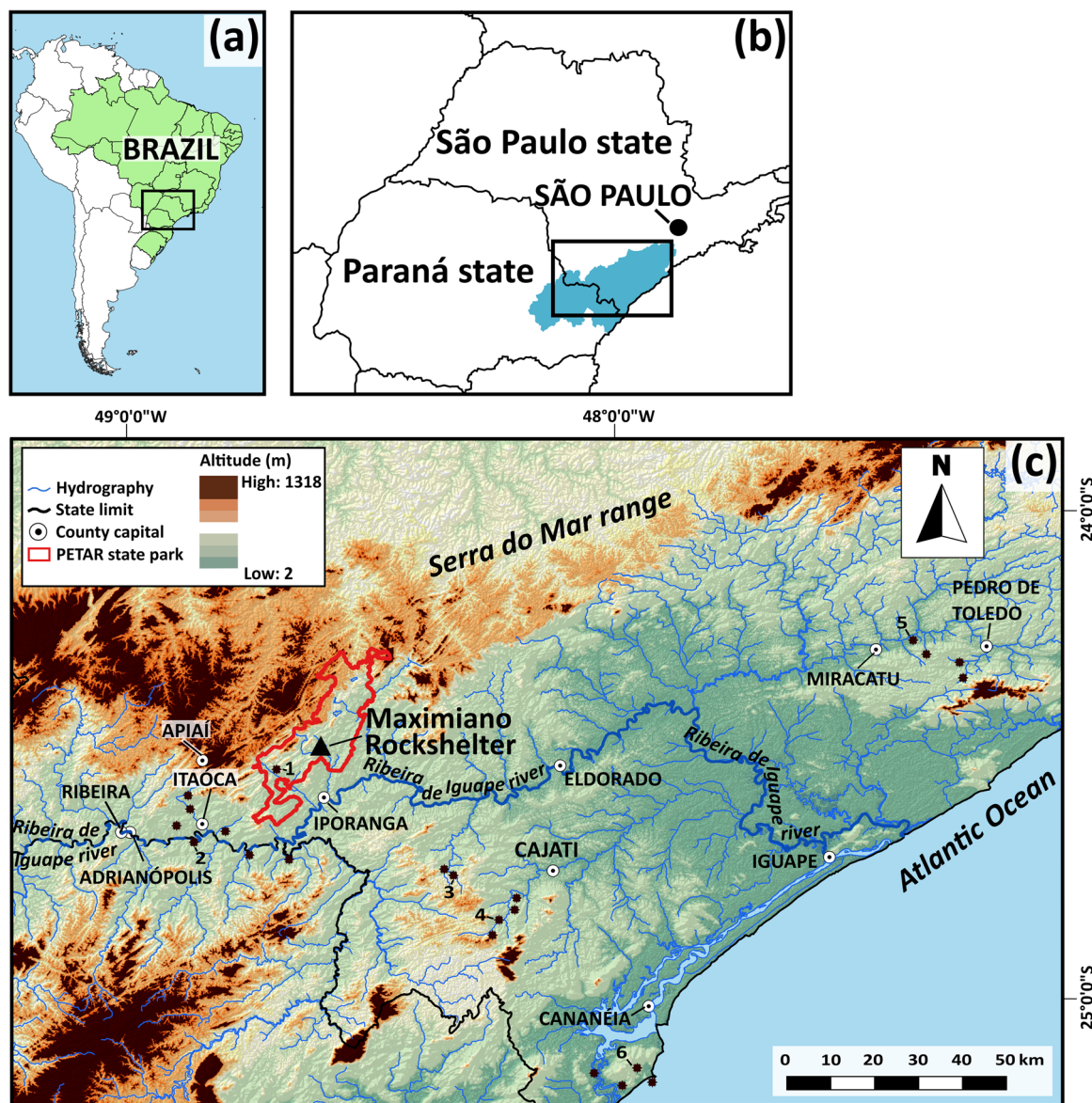


FIGURE 1 | (a) Map showing Brazil within South America, with (b) inset rectangular area highlighted. (b) Map showing the São Paulo and Paraná states, with the Ribeira de Iguape basin highlighted in sky blue and a rectangle exhibiting the extent of the main (c) map. (c) The Ribeira de Iguape basin with location of the Maximiano Rockshelter, main county capitals, geographic markers, and other archaeological sites mentioned in the text. 1: Morro Preto Cave; 2: Estreito riverine *sambaqui*; 3: Batatal I riverine *sambaqui*; 4: Capelinha I riverine *sambaqui*; 5: Moraes riverine *sambaqui*; 6: Cambriu Grande coastal *sambaqui*.

the Casa de Pedra, a 5547-m-long cave system (Fundação Florestal 2010), and measures 40 m long and 5 m wide. Its maximum height is 3 m at the dripline, and the present floor is ~6 m above the level of a small tributary of the Maximiano river which runs 11 m in front of the site. The shelter is surrounded by thick rainforest, with some plants occupying part of the plan area (Figure 2a,b).

A total of 17 m² of the site was first excavated by Collet and collaborators during two rapid and unsystematic field seasons in 1978 (Collet 1978a, 1978b). Collet's fieldnotes and interpretations were partly reported by himself (Collet 1978a, 1978b) and partly transcribed by Felizardo (2017, p. 139–148).

Collet's interventions consisted of 1 m² test pits or squares within four excavation Sectors (I–IV) (Figure 2c), while a fifth excavation area (Sector V), of unknown origin, is also

present at the site. A maximum depth of ~240 cm from the present-day surface was excavated in Sector II without reaching the bedrock. All the excavation sectors were left unfilled by Collet. The archaeological record observed and collected at the time comprised both knapped and ground lithic artifacts, bone points, faunal remains, and human bones (Collet 1978b). Human bones were recovered between 0 and ~120 cm below the surface, representing at least three primary burials (Felizardo 2017, p. 143–147). A human mandible, collected in Sector II at a depth of 180 cm, yielded a radiocarbon age of 9810 ± 150 B.P. (GIF7493) (Collet 1985), which at the time posited Maximiano as one of the earliest archaeological sites of southeastern Brazil.

Thirty-seven years after Collet's interventions, renewed archaeological work was carried out in 2015 and 2016 by a team from the

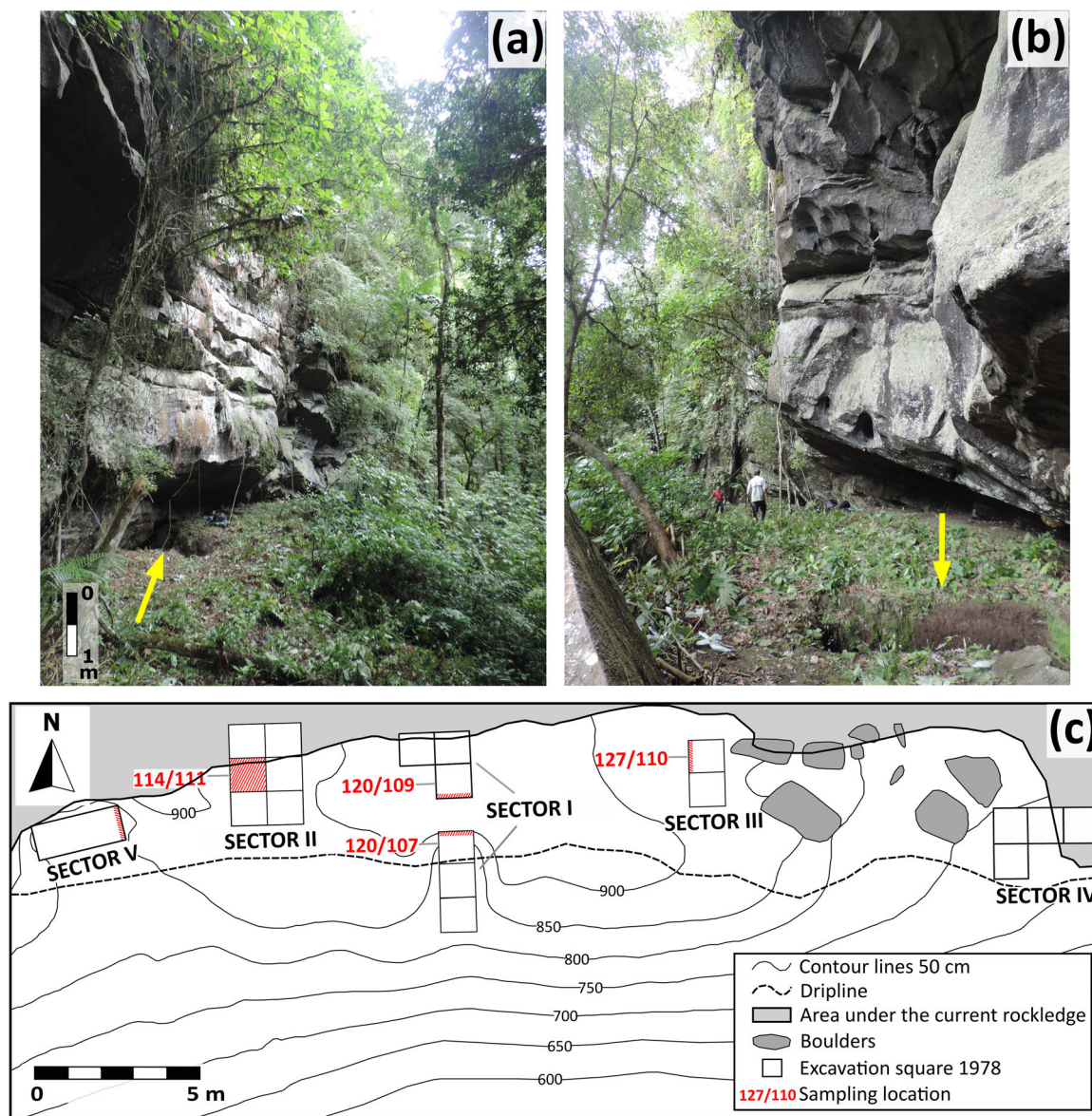


FIGURE 2 | (a) The Maximiano Rockshelter, as viewed from the southwest. The yellow arrow indicates part of excavation Sector II. Note dense rainforest vegetation. (b) Eastern view of the site, with yellow arrow pointing at excavation Sector III. (c) Plan of the site showing squares excavated by Collet and colleagues. Profiles and excavated surface sampled in this study are marked by red parallel oblique lines (modified from Collet 1978b and Felizardo 2017).

University of São Paulo. This work aimed to establish a chronology for the site, determine the depth of its cultural deposits, and produce a topographic map (Figure 2c; Araujo 2016; Felizardo 2017). Based on 15 calibrated AMS radiocarbon ages (Table 1), occupation was set at the end of the Early Holocene and mostly during the Middle Holocene. A human metatarsal recovered during profile rectification also posits a late Holocene occupation ca. 1395 B.P. (PSUAMS-4037). One charcoal sample yielded an unexpected age of ca. 1310 B.P. (Beta 432546), which is much younger than the overlying deposits (see Section 4.3). Excavation focused on Sectors I and II, because they were among the less affected by weathering, collapse, and bioturbation (e.g., armadillo burrows) and, in the former, because it was where the dated human mandible was recovered by Collet. Due to time and logistical restrictions, only a ~30-cm-thick sediment cover was excavated in Square 114/111—Sector II and a ~10-cm-thick one in Square 120/107—Sector I, without reaching either sterile layers or the bedrock (Felizardo 2017).

In November 2020, another field campaign was carried out specifically targeted at stratigraphy and sediment sampling to characterize site formation processes. The results of these activities are the focus of this article.

2 | Materials and Methods

To tackle the diversity of stratigraphic patterns observable at the site, a facies approach was implemented. Of widespread use in geoarchaeology, the facies concept groups bodies of sediment with shared physical attributes that can occur in different stratigraphic positions both within and between archaeological sites, with the aim of understanding depositional processes and human activities with common origins (e.g., Haaland et al. 2021; Karkanas and Goldberg 2018; Macphail et al. 1997; Miller et al. 2013; Villagran et al. 2021, 2009).

TABLE 1 | Radiocarbon ages obtained for the Maximiano Rock-shelter site.

Sample ID	Laboratory ID	Sector and square	Assigned facies	Sample type	Depth (cm)	¹⁴ C B.P. age	Cal range B.P., 95.4% probability (2σ) ^a	Reference
MAX-401	Beta 432546	Sector I South/Square 120/107	—	Charcoal	166.5	1310 ± 30	1273–1082	Felizardo (2017), this work
MAX-48	PSUAMS-4037	Sector II/Square 114/111	Intrusive	Human metatarsal	196.4	1395 ± 15	1301–1183	This work
MAX-367	Beta 432544	Sector I North/Square 120/109	F2a	Charcoal	21.5	6110 ± 30	7153–6796	Felizardo (2017), this work
MAX-406	Beta 432548	Sector II/Square 114/111	F16	Charcoal	198.3	6360 ± 30	7319–7164	Felizardo (2017), this work
MAX-358	Beta 432539	Sector III/Square 127/110	F11	Charcoal	61.4	6410 ± 30	7420–7171	Felizardo (2017), this work
MAX-366	Beta 432543	Sector I North/Square 120/109	F2a	Charcoal	55.0	6430 ± 40	7423–7176	Felizardo (2017), this work
MAX-360	Beta 432540	Sector I North/Square 120/110	—	Charcoal	48.0	6440 ± 30	7422–7260	Felizardo (2017), this work
MAX-361	Beta 432541	Sector I North/Square 120/110	—	Charcoal	91.7	6460 ± 30	7423–7273	Felizardo (2017), this work
MAX-362	Beta 432542	Sector I North/Square 120/110	—	Charcoal	19.9	6470 ± 30	7424–7278	Felizardo (2017), this work
MAX-414	Beta 432550	Sector II/Square 114/111	F16	Charcoal	204.3	6550 ± 40	7558–7323	Felizardo (2017), this work
MAX-408	Beta 432549	Sector II/Square 114/111	F16	Charcoal	201.4	6570 ± 30	7561–7332	Felizardo (2017), this work
MAX-423	Beta 432551	Sector II/Square 114/111	F16	Charcoal	208.0	6580 ± 30	7563–7338	Felizardo (2017), this work
MAX-402	Beta 432547	Sector II/Square 114/111	F16	Charcoal	195.1	7010 ± 30	7926–7696	Felizardo (2017), this work
MAX-357	Beta 432538	Sector III/Square 127/110	F12	Charcoal	85.2	7030 ± 30	7931–7713	Felizardo (2017), this work
MAX-370	Beta 432545	Sector I South/Square 120/107	F7	Charcoal	111.2	7880 ± 40	8974–8481	Felizardo (2017), this work
—	GIF-7493	Sector II/Square 114/112	—	Human mandible	180.0	9810 ± 150	11,712–10,699	Collet (1985)

^aCalibrated with the *rcarbon* (Crema and Bevan 2021) package in R (R Core Team 2021) using the SHCal20 atmospheric curve (Hogg et al. 2020).

The field characterization and sampling strategy took place in four of the stratigraphic profiles left exposed by Collet's excavations: south profile, Square 120/109 (Figure 3a,b); north profile, Square 120/107 (Figure 3c,d); west profile, Square 127/110 (Figure 4a,b); east profile, square of Sector V (henceforth, Square V) (Figure 4c-e). These profiles were selected because of their greater integrity and because they offer a generalized view of the main sectors of the site. Facies description was performed according to texture, sedimentary structures (e.g., lenses and <1-cm-thick laminae), Munsell color, visual estimation of gravel-sized artifactual, mineral and organic inclusions (e.g., shell fragments, charcoal), degree and shape of stratigraphic boundaries, and consistency when dry (Collinson et al. 2006;

Goldberg and Macphail 2006). Radiocarbon ages were calibrated with the *rcarbon* (Crema and Bevan 2021) package in R (R Core Team 2021) using the SHCal20 atmospheric curve (Hogg et al. 2020).

2.1 | Micromorphology

Nine undisturbed oriented sediment blocks were collected in the four stratigraphic profiles: blocks C, D, and E in south profile, Square 120/109 (Figure 3a); blocks A and B in the north profile, Square 120/107 (Figure 3c); blocks F, G, and H in the east profile, Square 127/110 (Figure 4a); block I in the west

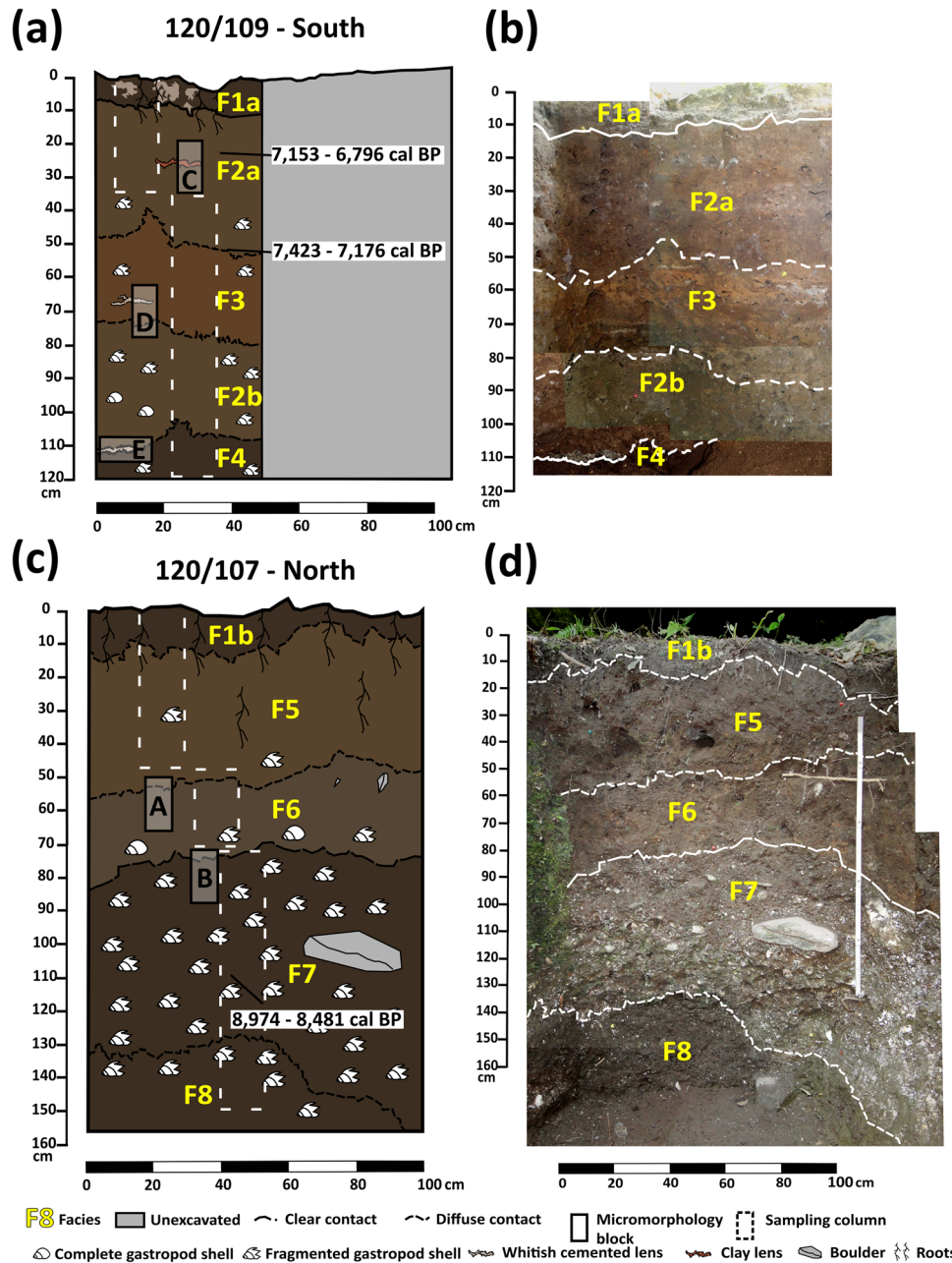


FIGURE 3 | Profiles sampled in Sector I. (a) Drawing of profile south, Square 120/109, showing both facies' names and location of micromorphological samples, sediment columns, and radiocarbon samples. (b) Photograph of profile drawn in (a) with facies identified. (c) Drawing of profile north, Square 120/107, with facies' names and location of micromorphological samples, sediment columns, and of radiocarbon sample obtained. (d) Photograph of profile drawn in (c) with facies identified. Two-sigma calibrated radiocarbon ages are extracted from Table 1.

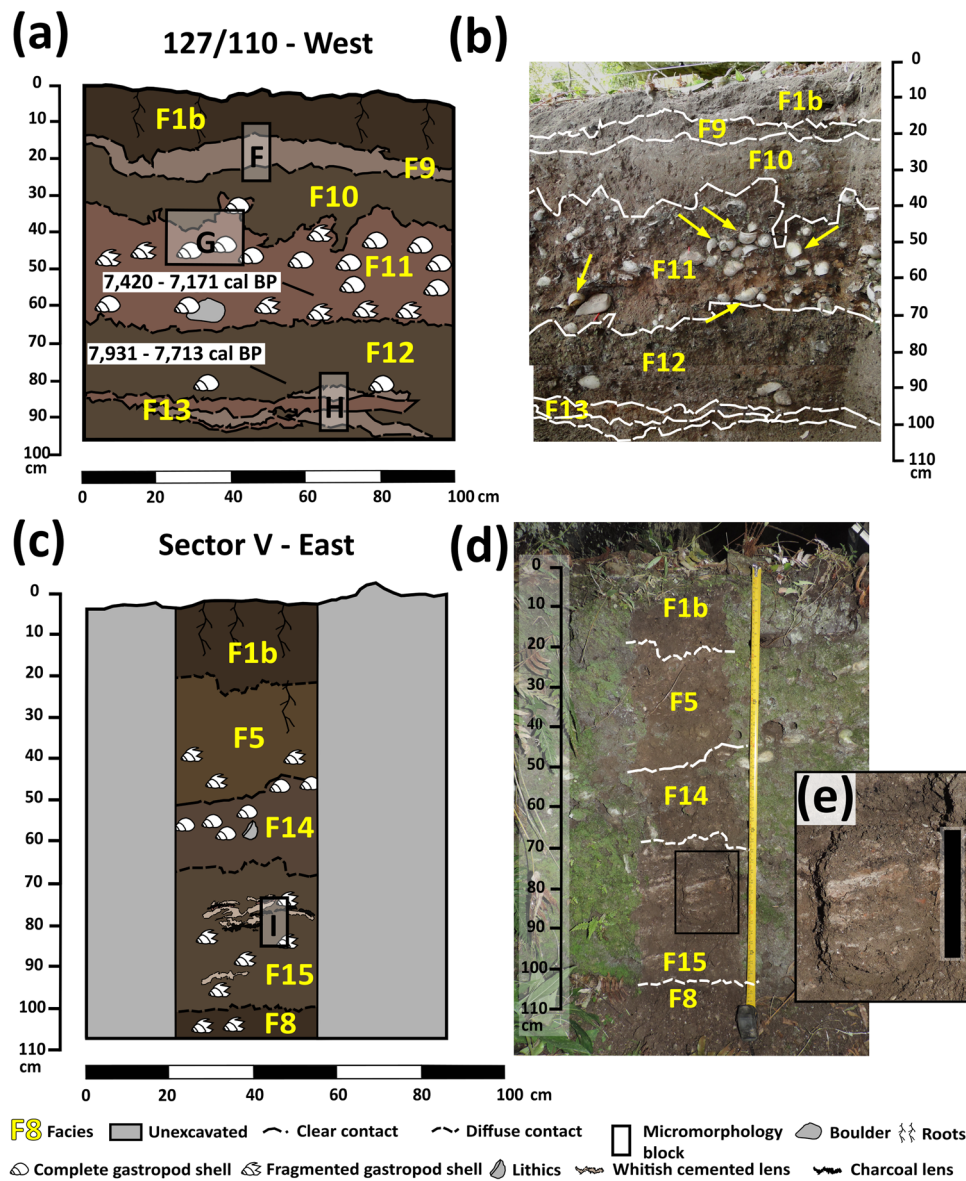


FIGURE 4 | Profiles sampled in Sectors III and V. (a) Drawing of profile west, Square 127/110, showing both facies' names and location of micromorphological and radiocarbon samples. (b) Photograph of profile drawn in (a) with facies identified. Yellow arrows show examples of complete shells of *Megalobulimus* spp. gastropods. (c) Drawing of profile east of the only square in Sector V, indicating facies' names and location of micromorphological sample I. (d) Photograph of profile drawn in (c) with facies identified. The rectangular inset highlights stratified lenticular layers within F15. (e) Detail of inset in (d), with alternating sediment lenses, black scale bar = 10 cm. Two-sigma calibrated radiocarbon ages are extracted from Table 1.

profile, Square V (Figure 4c). Extraction from the profiles was carried out mostly with cardboard boxes secured with cling film and parcel tape. In one case, plaster bandages were wrapped around a looser sediment monolith and left to dry to avoid its collapse (Goldberg and Macphail 2003).

Thin section production took place at the McBurney Laboratory for Geoarchaeology (University of Cambridge, UK) following French and Rajkovača (2015). After a period of air and oven drying totaling around 3 weeks, sediment blocks were impregnated with a solution of 1800 mL of polyester casting resin, up to 300 mL of acetone and ~4 mL of the catalyst methyl ethyl ketone peroxide (MEKP). Impregnated blocks were taken to a vacuum chamber for 24 h to remove the remaining bubbles. A top-up of the impregnation mix was added when necessary.

Once fully hardened, blocks were cut into 5-mm-thick slices and then ground in a Brot multiplate grinder. This stage involved a two-step mounting of the slices on 14 × 6.5 cm glass and grinding up to a thickness of ~30 μm.

Thin sections were scanned at LabMicro/MAE (University of São Paulo, Brazil) using different light sources in high resolution prior to analysis (Arpin et al. 2002; Goldberg and Aldeias 2018). Observations were made under magnifications ranging from ×7.25 to ×400 using a Leica Wild M420 macroscope and both a Leitz Laborlux 12 POL and an Olympus BX53 polarizing petrographic microscopes. Plane-polarized (PPL), cross-polarized (XPL), and oblique incident (OIL) light were the sources used for examination. Micromorphological descriptions followed standard guidelines (Bullock et al. 1985; Stoops 2021). Identification of

depositional and post-depositional components was based on soil/sediment micromorphology manuals (Stoops et al. 2018), as well as on archaeological micromorphology reference texts (Courty et al. 1989; Nicosia and Stoops 2017) and relevant case studies.

Microfacies (mF) were counted from top to bottom, following variation in consecutive layers and laminae. These were later grouped into microfacies types (mF types) (e.g., Haaland et al. 2021; Karkanas et al. 2015; Morrissey et al. 2023; Villagran 2019). Nomenclature procedures are explained in Supporting Information S1: Figure S1.

A scanning electron microscope (SEM) analysis was performed on one resin-impregnated block. Methods and results are included in Supporting Information S1: Text S1 and Supporting Information S1: Figure S2.

2.2 | Bulk Sample Analyses

The collection of bulk samples was aimed at obtaining a comparative view of physical and geochemical properties of deposits from the least and most exposed areas within the rock-shelter. Thus, only profiles in Square 120/109 (south) and Square 120/107 (north), both located in the central part of the site, were considered. Twenty-seven samples were collected following columns at 10-cm intervals (Figure 3a,c). Alongside these, samples from excavated plans in squares 120/107 ($n = 1$) and 114/111 ($n = 3$) were included in some of the analyses. For comparison with a background context, an off-site sample was collected ~34 m away to the northeast from the center of the sheltered area.

Sections 2.2.1 to 2.2.3 describe the main procedures employed. For statistical procedures, both the R programming language and the RStudio 1.4 environment (R Core Team 2021; RStudio Team 2020) were employed (see specific packages and references in Supporting Information S1: Text S1).

2.2.1 | Particle Size and Initial Parameters

The <1 mm sediment fraction was characterized by laser diffraction using a Malvern Mastersizer 2000 at the Technological Characterization Laboratory/University of São Paulo, Brazil (LCT/USP). To compare the terrigenous components of both the less and more exposed areas of the rock-shelter, both organic matter and carbonates were removed prior to analysis with 30% H₂O₂ and 10% HCl, respectively. Samples were dispersed into distilled water with two to five drops of 40% sodium hexametaphosphate. Grain-size frequencies were classified according to the Udden-Wentworth scale and size distributions analyzed following Pearson's moment measures (Swan et al. 1979).

Additional analyses (pH, organic carbon [OC] and carbonates) were carried out at the Soil Science Laboratory/University of São Paulo (LSO/USP) and at the Nuclear and Energy Research Institute, São Paulo (IPEN—CNEN/SP) to infer preservation conditions and biotic, and anthropogenic additions. Sediment pH was measured for

about 10 g of each sample, both in water and in KCl, with a 1:2.5 soil-to-liquid proportion (Teixeira et al. 2017). OC was determined using the Walkley-Black wet digestion procedure, modified after Camargo et al. (2009, p. 18–19). Carbonates were estimated from the inorganic carbon fraction using the loss-on-ignition (LOI) method detailed in Heiri et al. (2001). Only LOI values obtained at 950°C are reported here.

2.2.2 | Major Element Analysis and Instrumental Neutron Activation Analysis (INAA)

To evaluate the overall impact of human activities versus geogenic contributions, elements usually regarded as enhanced by both were measured. Semi-quantitative X-ray fluorescence (XRF) was conducted at LCT/USP on lithium tetraborate-fused glass beads of every sample using a Malvern PANalytical Zetium instrument to determine Al₂O₃, CaO, MgO, MnO, P₂O₅, SiO₂, and TiO₂. Available phosphorus (henceforth, av. P) and exchangeable ions Al³⁺, Ca²⁺, K⁺, and Mg²⁺ were also determined at LSO/USP. Av. P was extracted with a Mehlich-1 solution (0.05 M HCl and 0.0125 M H₂SO₄) and measured by colorimetry (after Teixeira et al. 2017). Principal component analysis (PCA) was employed to determine variables (elements) contributing to differences between the identified facies groupings (see Supporting Information S1: Text S4). INAA is a quantitative analytical technique that measures gamma rays emitted by radioactive atomic nuclei which are formed in samples irradiated with neutrons, usually in a nuclear research reactor (Bode 2017; Munita et al. 2019). Because of the simultaneous analysis of major, minor, and trace elements with high accuracy and precision, INAA has been widely used in both characterization and provenance analysis of pottery pastes and other archaeological materials (Glascok and Neff 2003; Bishop 2017). In this work, INAA was used to fingerprint shared geochemical behaviors by analyzing some major elements (K, Na) and others that generally occur in trace level in soils, for example, rare earth elements and Hf (Gallello et al. 2013; Sulas et al. 2019; Tudela et al. 2020).

Sediment samples were ground in an agate mortar, sieved using a 100-mesh sieve, oven-dried for 24 h at 105°C, and stored in a desiccator. Between 100 and 120 mg sediment aliquots were weighed in polyethylene containers. Sets of aliquots were irradiated alongside the standard material Constituent Elements in Coal Fly Ash, NIST-SRM-1633b. The candidate to certified reference material, RM-ISE 2015-1 International Soil-Analytical Exchange, Department of Environmental Sciences, Wageningen University, Netherlands, WE-PAL, was used for analytical quality control. Irradiation took place at the IEA-R1 nuclear research reactor of IPEN—CNEN/SP, Brazil, during 8 h at a thermal neutron flux of $1.21 \times 10^{12} \text{ n cm}^{-2} \text{ s}^{-1}$. Gamma-ray activity was measured with a Canberra GX2519 hyperpure Ge detector and associated electronics, the analysis of spectra being performed with Canberra's Genie 2000 software (more details in Munita et al. 2019, 2020). Both samples and standards were left to decay and counted after 5–6 days to measure K, La, Lu, Na, Sm, and Yb and after 25–30 days to determine Ce, Co, Cr, Cs, Eu, Fe, Hf, Sc, Ta, Th, and Zn. After analysis of precision of the reference material RM-ISE 2015-1, only the elements Ce, Co, Cs, Eu, Fe, Hf, K, La, Lu, Na, Sc, Th, and Yb were used for this study (see details in Supporting Information S1: Text S2 and Supporting Information S1: Table S1).

Multivariate statistical analyses targeted the detection and further exploration of distinct compositional groups behind facies variation (Glascock 2019). Hierarchical cluster analysis (HCA) was performed to find these groups (clusters) in an unsupervised manner by employing the k-means algorithm. Linear discriminant analysis (LDA), a dimensionality reduction technique that maximizes differences between groups by constructing discriminant functions (or linear discriminants), was used to validate the belonging of individual samples to their assigned clusters obtained via HCA.

2.2.3 | Fourier Transform Infrared (FTIR) Spectroscopy

FTIR spectroscopy has become one of the most widespread techniques for a fast and inexpensive characterization of inorganic and organic compounds in archaeological cave and rock-shelter deposits (e.g., Weiner et al. 2002; Friesem et al. 2021; Meinekat et al. 2022; Monnier 2018). In this work, it was also used to identify possible thermal alteration of clay minerals (Berna et al. 2007; Forget et al. 2015; Villagran, Strauss, et al. 2017; Ogloblin Ramirez et al. 2023). These analyses were developed at the McBurney Laboratory for Geoarchaeology (University of Cambridge).

Up to a few micrograms of every sample, previously ground in an agate mortar, were mixed with KBr powder to perform analysis in transmission mode following Weiner (2010), using a Thermo Scientific Nicolet iS5 FTIR spectrometer. Spectra were collected in the mid-infrared range, between 4000 and 400 cm^{-1} , recording 32 scans at a resolution of 4 cm^{-1} . A background spectrum was collected prior to every sample scan to control for the effect of water and carbon dioxide. The infrared library of the Kimmel Center for Archaeological Science, Weizmann Institute of Science, Israel (Weiner 2010), was consulted for spectra interpretation.

3 | Results

3.1 | Field Characterization and Micromorphological Analysis

In this section, the main macrostratigraphic patterns observed in the different profiles in the field are characterized, together with the microstratigraphic components. Presentation order roughly follows a chronological from-bottom-to-top sequence. A total of 16 facies were recognized (Table 2). The diversity and frequency of gravel-sized components (the most conspicuous being the gastropod shells), textural differences between sectors, and the presence of both massive and lenticular mm-sized laminae or cm-sized layers all indicated a high variability of stratigraphic patterns. This variability was also mirrored in the microscopic scale. Within the nine thin sections analyzed, 32 mF were identified and grouped into 14 mF types (Table 3, Tables S1–S5).

3.1.1 | Dark Basal Deposits of the More Exposed Areas: Square 120/107 and Sector V

These comprise F8, organic sand clayey very dark brown deposits with frequent shell fragments found at the bottom of profiles north of Square 120/107 (Figure 3c,d) and west of Square V (Figure 4c,d), in direct contact with the unexcavated surfaces. No

micromorphological blocks were collected in this facies. Preliminary analysis of the materials recovered in the < 2 cm fraction of the ~10-cm-deep excavation carried out in this layer in 2016 indicated the presence of both artifacts and pebbles of quartz and metamorphic rocks, bones of birds, marsupials and Xenarthra, and human bones (Felizardo 2017, p. 120). The unexpected young age of ca. 1310 B.P. was obtained for this deposit in Square 120/107 (Table 1), likely the result of chemical contamination (see Section 4.3).

3.1.2 | Shell Fragment-Supported Deposit: Square 120/107

It consists of F7, a shell-rich 67-cm-thick deposit in the mid-to-lower portion of profile north of Square 120/107, which stands out for the presence of more than 50% closely packed gastropod shell fragments among other gravel-sized inclusions (Figure 3c,d). A radiocarbon age of between 8974 and 8481 cal B.P. (Beta 432545) was obtained for this layer, thus being the oldest date available for the site after the one reported by Collet (1985) (see Table 1).

The contact between the top of this layer and the bottom of the sandy loam F6 was sampled for micromorphology in block B (Figure 5b,c). Characterized as mF type 7b, the latter exhibits mostly sand-size grains bridged by humic material and clay (see Supporting Information S1: Figure S3 and Section 4.3). The former is microstratigraphically recognized in mF type 8a, a sediment of excremental microaggregate matrix, supported mostly by shell fragments in subvertical orientation and a mixture of diverse anthropogenic constituents (Figure 5c,f,g), which include lithic knapped artifacts (Figure 5c,f) and fire-derived/exposed materials. Apart from charcoal, evidence for burning came from cm-sized subrounded aggregates (Figure 5c) of mostly reprecipitated calcitic ash crystal pseudomorphs (which preserve the form of the original calcium oxalate crystals present in plant tissues, see Canti 2003; Canti and Brochier 2017), heated shell fragments (Figure 5f), and bones (Figure 5i), which would have been exposed to different temperatures ranging between 500°C and 900°C (after experimental data from Villagran, Huisman, et al. 2017).

3.1.3 | Bedded Lenticular Sequences: Square 127/110 and Square V

These include two distinct layers in the east (Square 127/110, west profile) and west (Square V, east profile) parts of the shelter, in which clear stratigraphic successions of both laminae and a few cm-thick lenticular layers occur. In the first case, clayey whitish and reddish layers alternate with each other in a 10-cm-thick sequence denominated F13, in contact with the unexcavated surface of the square (Figure 4a,b). In the second case, the F15 sequence (Figure 4c,d) of ~37 cm in thickness consists of macroscopic indurated thin whitish laminae and lenses which vertically succeed others which are dark, charcoal-rich, and reddish clayey (Figure 4e). This sequence overlies the dark deposits assigned to F8. Absolute chronological data are available only for the F13 to F12 transition, which yielded an age of 7931 to 7713 cal B.P. (Beta 432538).

Both bedded sequences were microstratigraphically characterized in thin sections H and I, made from blocks, respectively, collected in

TABLE 2 | Description of facies characterized in the Maximiano Rockshelter site.

Facies	Depth (cm)	Field description
F1a	0–10 (Square 120/109)	Organic silty clay, very dark brown (10YR 2/2) soft matrix, with common distinct pinkish gray mottles (7.5YR 6/2). Sharp and wavy lower contact. Includes many roots.
F1b	0–12 (Square 120/107) 0–20 (Square 127/110) 0–23 (Square V)	Organic silty, very dark brown (10YR 2/2) soft matrix. Gradational and wavy lower contact. Includes many roots. It exhibits characteristics of a soil A horizon.
F2a	10–50 (Square 120/109)	Silt loam with lenticular cm-sized layers reddened clayey sediment, dark brown (10YR 3/3) soft matrix, with gastropod shell fragments (7%), sub-rounded aggregates of rubified clayey sediment < 1 cm (7%) and charcoal (7%–10%). Gradational and irregular lower contact. Few roots.
F2b	78–105 (Square 120/109)	Silt loam with lenticular cm-sized layers of whitish sediment, dark yellowish brown (10YR 3/4) slightly hard matrix, with complete gastropod shells (3%) and shell fragments (15%), sub-rounded aggregates of rubified clayey sediment < 1 cm (3%) and charcoal (10%). Gradational and irregular lower contact.
F3	50–78 (Square 120/109)	Sand clay with lenticular mm-to-cm-sized layers of whitish sediment, dark brown (7.5YR 3/4) slightly hard matrix, with gastropod shell fragments (15%), aggregates of rubified clayey sediment > 1 cm (10%) and charcoal (10%). Gradational and irregular lower contact.
F4	105–120 (Square 120/109)	Silt loam with lenticular cm-sized layers of whitish cemented sediment, some cemented, very dark brown (10YR 2/2) slightly hard matrix, with gastropod shell fragments (15%), sub-rounded aggregates of rubified clayey sediment < 1 cm (5%) and charcoal (10%).
F5	12–45 (Square 120/107) 20–50 (Square V)	Loam, dark brown (10YR 3/3) soft matrix, with gastropod shell fragments (7%), sub-rounded aggregates of rubified clayey sediment < 1 cm (5%) and charcoal (3%). Gradational and wavy lower contact. Roots are common.
F6	45–83 (Square 120/107)	Sandy loam, very dark grayish brown (10YR 3/2) soft matrix, with complete gastropod shells (5%) and shell fragments (20%), pebbles/lithic artifacts (3%), sub-rounded aggregates of rubified clayey sediment > 1 cm (3%) and charcoal (3%). Clear and wavy lower contact.
F7	83–150 (Square 120/107)	Bioclast-supported (> 50% bioclasts) deposit with a sand clay hard matrix, very dark brown (10YR 2/2) matrix, hard, enriched in gastropod shell fragments (> 50%), with pebbles/lithic artifacts (3%) and charcoal (2%). Clear and wavy lower contact.
F8	130–170 (Square 120/107) 100–105 (Square V)	Organic sand clay, very dark brown (10YR 2/2) soft matrix, with gastropod shell fragments (20%) and charcoal (5%).
F9	15–25 (Square 127/110)	Sand clayey loam, grayish brown (10YR 5/2) hard matrix, with gastropod shell fragments (3%) and charcoal (10%). Clear and wavy lower contact.
F10	20–40 (Square 127/110)	Sandy loam, very dark grayish brown (10YR 3/2) slightly hard matrix, with gastropod shell fragments (10%), sub-rounded aggregates of rubified clayey sediment < 1 cm (2%) and charcoal (5%–20%). Clear and irregular lower contact.
F11	35–65 (Square 127/110)	Sandy loam matrix-supported bioclastic (45% bioclasts) deposit, reddish brown (2.5YR 4/3) soft matrix, with complete (25%) and fragmented (20%) gastropods, lithic artifacts (2%) and charcoal (3%). Clear and wavy lower contact.
F12	65–95 (Square 127/110)	Loam, very dark grayish brown (10YR 3/2) slightly hard matrix, with complete (3%) and fragmented (10%) gastropod shells, sub-rounded aggregates of rubified clayey sediment < 1 cm (2%) and charcoal (20%).
F13	85–95 (Square 127/110)	Alternating silt-loam- to- sand-clayey succession of lenticular mm-to- cm-sized layers of whitish cemented and reddened clayey sediment, reddish brown (2.5YR 4/3) to reddish gray (5YR 5/2), with charcoal (10%). Clear and wavy lower contact.
F14	42–63 (Square V)	Sand clay loam matrix-supported bioclastic (20% bioclasts) deposit, dark brown (7.5YR 3/2) slightly hard matrix, complete (15%) and fragmented (5%) gastropod shells, pebbles/lithic artifacts (1%) and charcoal (10%). Gradational and wavy lower contact.

(Continues)

TABLE 2 | (Continued)

Facies	Depth (cm)	Field description
F15	63–100 (Square V)	Alternating succession of lenticular mm-to-cm-sized layers of whitish shelly, charcoal-rich, and reddened clayey sediment, enclosed by a dark brown (7.5YR 3/2) sand clay loam slightly hard matrix, with gastropod shell fragments (30%), aggregates of rubified clayey sediment < 1 cm (7%) and charcoal (10%). Clear and wavy lower contact.
F16	180–210 (114/111)	Silt loam, dark brown (7.5YR 3/4) soft matrix, with gastropod shell fragments (3%), sub-rounded aggregates of rubified clayey sediment > 1 cm (3%) and charcoal (5%).
EF1	10–20	Clay loam to sand clay, dark olive-gray (5Y 3/2) hard matrix. Gradational lower contact. Includes many roots. Upper horizon of the immediate off-site soil.

F13 and F15. Under the microscope, F13 revealed to be a stacked succession of discrete layers/lenses of ash crystals in a sparry calcite-rich micromass (mF type 4b), mostly crystallitic in XPL (Figure 6a,g,h), and of accumulations rich in reddened clay with ashes (mF types 12a and 12c, Figure 6a,c,d,e). A less porous undulating sequence of laminated cemented ash alternated by articulated ashes (in anatomical position), partially carbonized tissues, and charcoal, is diffusely bounded underneath the third ash layer from the bottom of the thin section (Figure 6a,f,i,j). This whole undulating sequence rests upon a laminar reddened clay deposit (mF type 12b, Figure 6a,f). Heated materials, like bones and shells, are ubiquitous in both ash-rich and clay-rich microfacies (Figure 6c,d). Two striking characteristics of shell fragments were observed, namely, that most of them are thicker than in the rest of the site (one of them being from a complete bivalve) and that they follow a horizontal orientation referred to the actual surface (Figure 6b).

A more complex microstratigraphic scenario was observed in F15. Here, cemented ash-derived laminae and lenses (mF type 14a and b), rich in shell fragments, are overlaid by banded subhorizontal shell fragments mixed with charcoal and rich in both charred organic material and burnt bones (mF type 13) (Figure 7a,b,e,f,g). Shells within these bands commonly exhibit in situ cracking, the different affected fragments being interconnected (Figure 7c,d,h). Both charcoal fragments and the organic-rich micromass immediately underneath these shells form angular blocky peds and plates separated by intersecting planes (Figure 7d). The succession of mF types 13 and 14a,b, totaling four laminae/layers, rests upon and it is overlaid by matrix-supported subvertical shelly deposits (mF type 8b), which present burnt (up to 400°C) and unburnt bones (Figure 7i,j). At the base of the thin section, there is a layer of matrix-supported subhorizontally oriented shell fragments (mF type 10d, Figure 7a,b), similar to others encountered in F11 (see Section 3.1.5).

3.1.4 | Loamy Deposits of the More Sheltered Area: Square 120/109

These consist of the four dm-sized massive layers identified in profile south of Square 120/109, from F4 at the bottom, through to F3, F2b, and up to F2a, in sharp contact with the top layer assigned to F1a (Figure 3a,b). A dark-colored silt loam texture characterizes all these facies but F3, which is more sand-rich. The deposits excavated in Square 114/111 (Sector II) in 2016,

also in the more sheltered area, exhibit similar macroscopic characteristics and were grouped under F16. These are the best dated deposits of the site, with an age for F16 of 7926 to 7696 cal B.P. (Beta 432547) and further 11 ages closely succeeding one another and ranging from 7563 to 6796 cal B.P. (Table 1). Despite the lower deposits (F16) having been excavated at a depth of ~180 cm from the surface, underneath Collet's interventions, they yielded much younger ages than the one obtained by him (11,712 to 10,699 cal B.P.; GIF-7493). Differences in datum location, as well as the fact that the precise stratigraphic provenience of the human mandible used to obtain that date is not known, may explain this discrepancy.

Microscopic examination undertaken in thin sections C and D (Figure 8a,d), produced from respective blocks sampled in F2a and transition F3/F2b, showed a similar random array of fine sand-sized-to-gravel-sized quartz grains and materials related to heat exposure, such as charcoal, burnt bones, and shell fragments (Figure 8b,c,g,h,i,j). A mostly secondary micrite-rich granular and porous crumb microstructure with clay characterizes the matrix of mF types 1a and 1b (Figure 8b,c). Discrete ash crystals frequently occur both in different random sectors and inside dense subrounded aggregates in which reprecipitated ashes predominate, these being larger in mF type 1b (Figure 8d,e,f). The presence of long straight and zigzag planes not separating clear major peds (only small subangular blocks) is a difference between mF types 1a and 1b (Figure 8d). A lamina composed of subrounded aggregates of clay of different sizes comprises mF type 2 (Figure 8a).

A similar groundmass was observed in thin section E (Figure 9a,b), which covers the basal F4 to F2b contact. However, unlike thin sections C and D, both the upper and lower-most microfacies of E exhibit a clearly pedalized structure, with mostly internally porous subangular blocks of different sizes (mF type 3). Another difference resides in these aggregates being more organic-rich, with common amorphous organic matter and comminuted silt-sized charcoal in the micromass (Figure 9a,c). A distinct sequence of a charcoal lamina/layer (mF type 5) superimposed by an ash-rich cemented lenticular layer (mF type 4a) was observed in a sharp transition with the subrounded aggregates at the bottom and top of thin section E (Figure 9b). Despite the sequence having been strongly affected by Fe oxide/hydroxide impregnation, articulated ashes in anatomical position were recognized within the cemented ash lens (Figure 9f,g,h). This lens presents a dark brown top with a platy

TABLE 3 | Microfacies types identified in the Maximiano Rockshelter, with a brief description of micromorphological attributes and the macro and mesostratigraphic position in which they were recognized.

mF type ID	Generic name	Main micromorphological characteristics	Stratigraphic context (thin section (square)—facies fabrics from top to bottom)
1a	Burnt materials mix	Granules and crumbs (up to 500 μm) to micro-aggregated micritic and clayey matrix, with abundant silt-sized charcoal and organic matter inclusions. Ash rhombs are randomly distributed in the micromass, but subrounded aggregates of reprecipitated ashes also occur. Apart from the predominant quartz grains (~30%), charcoal (30%), clay aggregates and gravel-sized sub-rounded bones are frequent, 15%–20% of the latter being burnt. Few random shell fragments occur, some of them with evidence of heat exposure.	Section C (120/109)—2a.1 and 2a.3
1b	Burnt materials mix, blocky	Similar coarse fraction and micromass composition to mF type 1a, but with few sub-angular blocks, weakly separated by planes. Reprecipitated ashes coalesce in subrounded 1-to-7 mm vughy aggregates.	Section D (120/109)—3.1
2	Clay layer	Lamina (< 1 cm) to 3-cm-thick layer of dark reddish brown subrounded clay aggregates with few quartz grains and charcoal as inclusions.	Section C (120/109)—2a.2
3	Organic ashy blocky	Granules to subangular highly separated cm-sized aggregates of similar composition and inclusions as mF types 1a and 1b. Shell fragments are now frequent.	Section E (120/109)—2b.1 and 4.3
4a	Ashes/cemented ash layer	A 2.5-cm-thick layer of Fe oxide/hydroxide-stained cemented ashes, with presence of articulated ashes in different sectors. It exhibits a dark brown Fe-oxidized top with a slightly jagged aspect produced by planar voids perpendicular to the main axis, at times filled with shell fragments.	Section E (120/109)—4.1
4b	Ashes/recrystallized ashes layer	Ash crystals and recrystallized ashes in a 1.5-to-1-mm- thick sparitic/microsparitic and clayey subangular blocky to interconnected vughy and spongy accumulation. Charcoal (30%), reddened clay subrounded aggregates (20%–30%, 100 μm to 3 mm in size), bones (20%), ~15%–20% of them burnt, and shell fragments occupy the coarse fraction. Some phosphatization and localized void coatings and infillings are observed.	Section H (127/110)—13.1, 13.3, 13.6, and 13.8
5	Charcoal layer	A lenticular, at times undulating layer of oxidized and humidified charcoal, underneath the ash layer mF type 4a.	Section E (120/109)—4.2
6	Organic-rich, loose	Excremental granular to intergrain micro-aggregate matrix, at times forming subangular blocks, with subrounded to subangular fine to medium sand-sized quartz (25%–30%) and occasional feldspar grains. Less than 20% of shell fragments and bones are present in random distribution.	Section A (120/107)—5
7a	Organic-rich, dense	Similar to mF type 6 in micromass and coarse fraction composition, but with a predominating	Section A (120/107)—6.1

(Continues)

TABLE 3 | (Continued)

mF type ID	Generic name	Main micromorphological characteristics	Stratigraphic context (thin section (square)—facies fabrics from top to bottom)
7b	Organic-rich, sandy	spongy microstructure alongside granules and blocks. Loose continuous infillings of fecal pellets are common inside channels and chambers. Excremental as mF type 7a, but more porous, the quartz grains being commonly bridged by humic organic matter and dirty clay.	Section B (120/107)—6.2
8a	Shell mix	Clast-supported organic intergrain micro-aggregated to subangular blocky matrix, with up to 1.5-cm-long subvertical shell fragments as the main (35%–45%) coarse component, alongside fine-sized quartz grains. Randomly distributed unburnt (20%) and burnt bones (15%), charcoal (5%–10%), subrounded clay aggregates (10%), reprecipitated ash aggregates (1%–2%) and some gravel-sized lithic artifacts (1%–2%) make up the suite of coarse anthropogenic inclusions.	Section B (120/107)—7
8b	Sparse shell mix	Similar to mF type 8a, but matrix-supported and with a predominant subangular blocky microstructure.	Section I (Square V)—15.1 and 15.6
9	Charcoal-rich, loose	Accumulation of loose organic and micritic granules, crumbs, and cm-sized subrounded aggregates, with fine-sand-sized quartz grains and charcoal as the predominant components of the coarse fraction (30%), it also includes shell fragments (5%–10%). These components are observed as being detached from the underlying layer (grouped into mF type 10a).	Section F (127/110)—9
10a	Subhorizontal shell mix	Subhorizontal shell fragments (15%–20%) in a moderately to highly separated subangular blocky (3–38 mm) micritic and clayey matrix, with straight and zigzag planes. A 2.5 × 1 cm-long angular calcareous rock fragment and a complete gastropod shell stand out in the coarse fraction, together with subangular fine sand-sized quartz grains, bones, and charcoal. The same shape and degree of alteration of quartz grains observed within rock fragments is present in the groundmass grains.	Section F (127/110)—10.1
10b	Subhorizontal shell layer	Openly packed and subhorizontally to horizontally distributed gastropod shell fragments (30%) interspersed in a micromass of the same composition as mF type 10a, also with subangular blocky peds separated by straight planes but less frequent.	Section G (127/110)—10.2
10c	Subhorizontal shell layer, loose	Same as mF type 10b, but with a more granular microstructure.	Section G (127/110)—10.3
10d	Subhorizontal shell layer, organic	Same as mF types 10b and 10c, but more organic and shell fragments are more frequent.	Section I (Square V)—15.7
11	Complete shell	Closely packed complete gastropod shells (40%) surrounded by subhorizontal and subvertical shell fragments (20%–30%). Inside the sectioned shells	Section G (127/110)—11

(Continues)

TABLE 3 | (Continued)

mF type ID	Generic name	Main micromorphological characteristics	Stratigraphic context (thin section (square)—facies fabrics from top to bottom)
		there is a moderately sorted very fine- to fine-sand-sized single quartz grain to locally organic, micritic, and clayey micro-aggregated matrix, with few (2%–5%) shell fragments, bones (5%), some of them burnt, and charcoal (2%).	
12a	Reddened clay accumulation	Accumulation of small (~50–100 µm) crumbs and granules, locally forming subrounded to vughy subangular 100-µm- to 2.5-mm-wide aggregates, composed of reddish-brown clay and ashes. Shell fragments (20%–30%), mainly thicker than the ones present in the rest of the site (probably from bivalve shells) and some of them (20%) exhibiting traces of heating, are mostly in a subhorizontal orientation. Alongside these, burnt bones (20%–30%) make up the coarse fraction.	Section H (127/110)—13.2 and 13.5
12b	Reddened clay lamina	A thin (500 µm-to-5 mm-thick) lenticular layer of vughy. Coarse fraction constituents are in the same frequency as in mF type 12a.	Section H (127/110)—13.4
12c	Reddened clay accumulation, loose	As mF type 12a, but more porous (vughs to complex packing voids).	Section H (127/110)—13.7
13	Subhorizontal/horizontal shell and charcoal	Bands of closely packed subhorizontally to horizontally distributed shell fragments (35%–45%), up to 2.3 cm long each, some of them interconnected after being cracked, interspersed in an organic and charred material-rich micromass. Partially dissolved charcoal fragments (30%) follow a subhorizontal to inclined orientation referred to the shell fragments. Few rock fragments and bones are present.	Section I (Square V)—15.2 and 15.4
14a	Ash and shell	A lenticular, massive to locally subangular blocky layer (~2 cm thick) of secondary micrite, ash crystals, and organic matter. It includes mostly mm-sized shell fragments in subhorizontal distribution (30%–40%), charcoal (25%–30%), and burnt bones (15%–20%).	Section I (Square V)—15.3
14b	Ash and shell with clay aggregates	Similar to mF type 14a, but thinner (mm-to-cm-sized) and with frequent subrounded clay aggregates (~300 µm to mm-sized).	Section I (Square V)—15.5

and slightly jagged aspect produced by planar voids perpendicular to the main axis (Figure 9b,d,e).

3.1.5 | Subhorizontal Matrix-Supported Shell Layers:

Square 127/110 and Square V

These include sandy loam matrix-supported layers which stand out for the presence of gastropod shells, both complete and as fragments, which tend to follow a subhorizontal orientation referred to the present-day surface. They were observed in the eastern (F10 and F11) and western (F14) sampled profiles (Figure 4a–d), on top of F12 in the former case and of the

stratified lenticular sequence F15 in the latter. A radiocarbon age of 7420 to 7171 cal B.P. (Beta 432539) was obtained for F11.

Micromorphological analysis was carried out of the F11 to F10 transition in thin sections G and F (Figure 10a,f,g). The sequence exhibits, at the base, a layer of complete gastropod (*Megalobulimus* spp. and *Thaumaustus* spp.) shells with subhorizontal shell fragments, charcoal, and burnt bones in between (mF type 11), which is overlaid by massive layers of upwardly increasingly less abundant shell fragments (mF types 10c to 10a) that have the same predominant orientation. Matrix composition is like the one observed in mF types 1a and 1b but with a more clayey, micrite-rich micromass (Figure 10b,h). The presence of subangular blocky peds separated by partially accommodated planes at the top of F10 (mF type 10a,

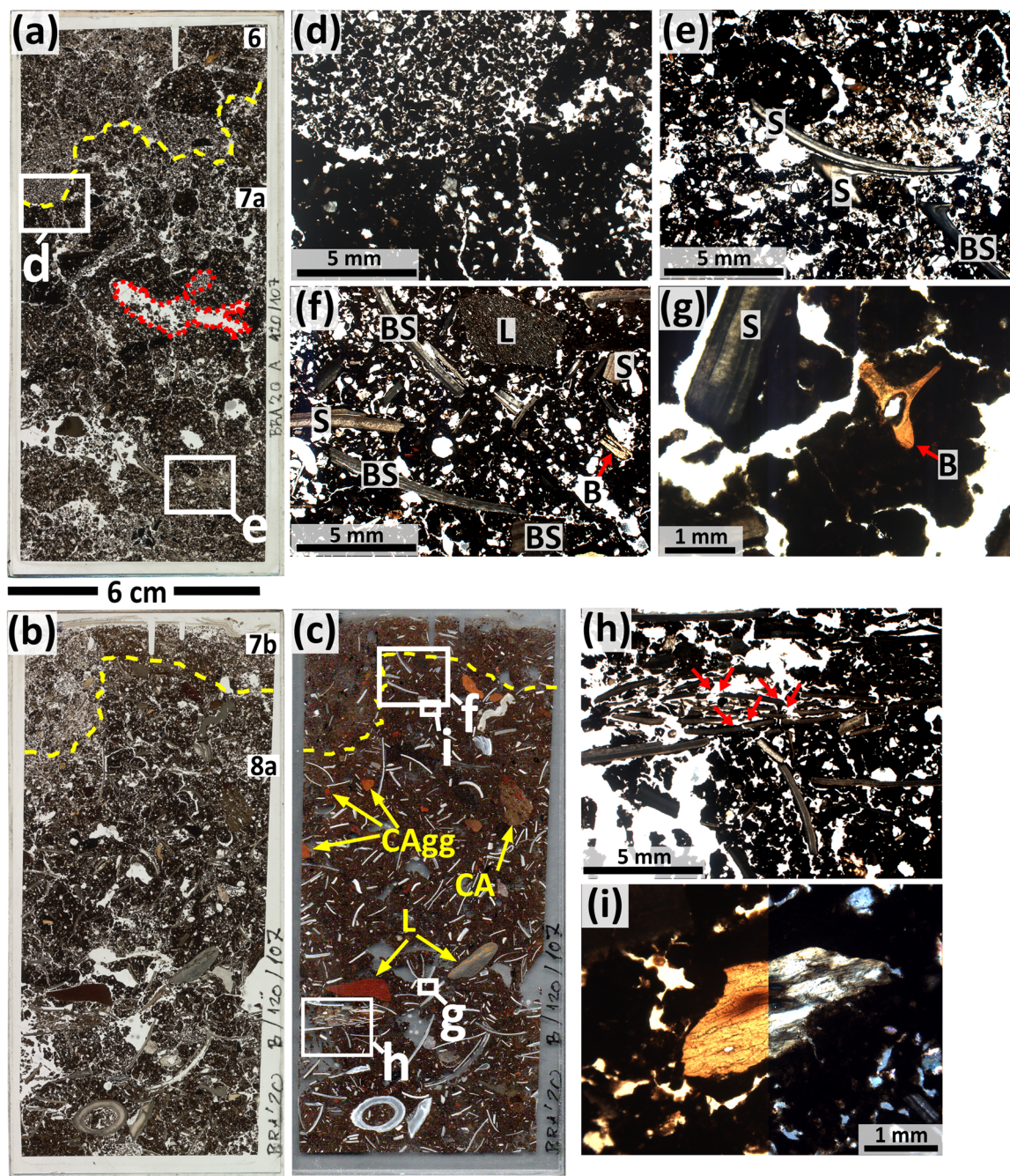


FIGURE 5 | Micromorphology samples A and B, collected in Square 120/107. (a) Thin section scan of sample A, in PPL, with microfacies types (6 and 7a) and sectors where photomicrographs were taken. Note the highly humified aspect. The red dotted line marks a channel infilled with loose excrements. (b) Thin section scan of sample B in PPL, with microfacies types (7b and 8a). (c) Dark-field thin section scan of sample B, with sectors where photomicrographs were taken. Apart from randomly distributed subvertical shell fragments in white, clay aggregates (CAGg), an aggregate of cemented ashes (CA) and lithic artifacts (L) are shown. (d) Photomicrograph of the contact between mF types 7a and 6, in PPL, the former exhibiting a denser groundmass. (e) Photomicrograph of mF type 7a, in PPL, showing shell (S) and burnt shell fragment (BS) amid a spongy organic microstructure. (f) Photomicrograph of mF type 8a, in PPL, which exhibits a random mix of shell fragments both unheated (S) and burnt (BS), bones (B), and a knapped lithic artifact (L). (g) Photomicrograph detailing a fish vertebra (B) and part of a shell fragment (S) in mF type 8a. (h) Photomicrograph of sector with interconnected shell fragments (red arrows) in mF type 8a. (i) Burnt bone fragment in mF type 8a, in PPL (left) and XPL (right). PPL, plane-polarized light; XPL, cross-polarized light.

Figure 10a) points out to a shrink–swell-affected clay matrix (Kovda and Mermut 2018). Most quartz grains show the same surface alteration present within angular gravel-sized carbonate rock fragments (Figure 10a,d,e) seemingly detached from the shelter's host rock (roofspall), which are encountered in thin section F.

3.1.6 | Loose Charcoal-Rich Layers: Square 127/110

This consists of F9, a cm-sized loose sandy loam layer which rests upon the shell-rich F10 in Square 127/110 (Figure 4a,b). Charcoal is the dominant gravel-sized component among

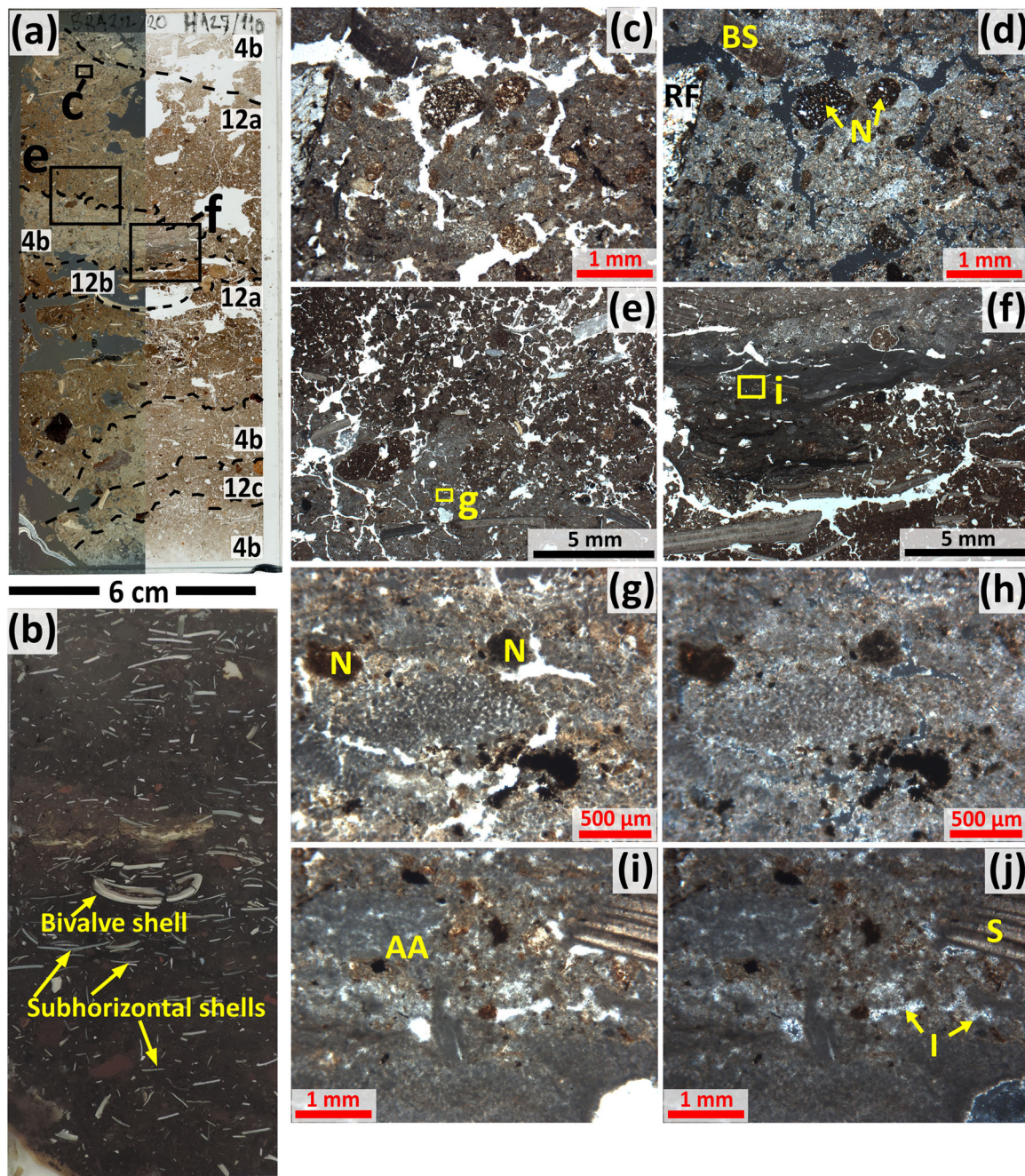


FIGURE 6 | Micromorphology sample H, collected in Square 127/110. (a) Thin section scan in PPL (right half) and XPL (left half), indicating alternating microfacies types (4b, 12a, 12b, and 12c) and sectors where photomicrographs were taken. Some areas were erased during section manufacturing. (b) Photo of impregnated block. Subhorizontally distributed shell fragments and a bivalve shell are highlighted. (c) Photomicrograph of mF type 12a, in PPL. Note the clayey and calcitic-rich micromass. (d) Same as (c) in XPL, note a mostly crystallitic microsparitic b-fabric, a rock fragment (RF), a burnt shell fragment (BS), and iron nodules (N). (e) Example of contact of mF types 4b (base) to 12a (top). The difference between a massive/subangular blocky microstructure in the former and a crumb one in the latter is clearly visible. (f) Detail of contact of the base of the main mF type 4b ash lens with the clay lamina mF type 12b. A laminated undulating sequence of cemented ashes and charcoal is visible at the center. (g) Detail of rectangle (g) in photomicrograph (e), showing discrete ash pseudomorphs and iron nodules (N). (h) Same as (g) in XPL. (i) Detail of rectangle (i) in micrograph (f) with example of articulated ashes. (j) Same as (i) but in XPL. Note recrystallization, microsparitic infillings (I) in voids and shell fragment (S). PPL, plane-polarized light; XPL, cross-polarized light.

shell fragments and others (Figure 10c). Under the microscope, these constituents, alongside the frequent crumbs/granules and common subrounded aggregates that make up the microstructure of mF type 9, are seen detaching from the underlying microfacies (mF type 10a) (Figure 10b).

3.1.7 | Dark Middle and Top Layers

Included here are F1a and F1b, the very dark brown massive organic root-rich loam layers that make up the top of all the studied profiles (Figures 3 and 4), and F5, the dark brown

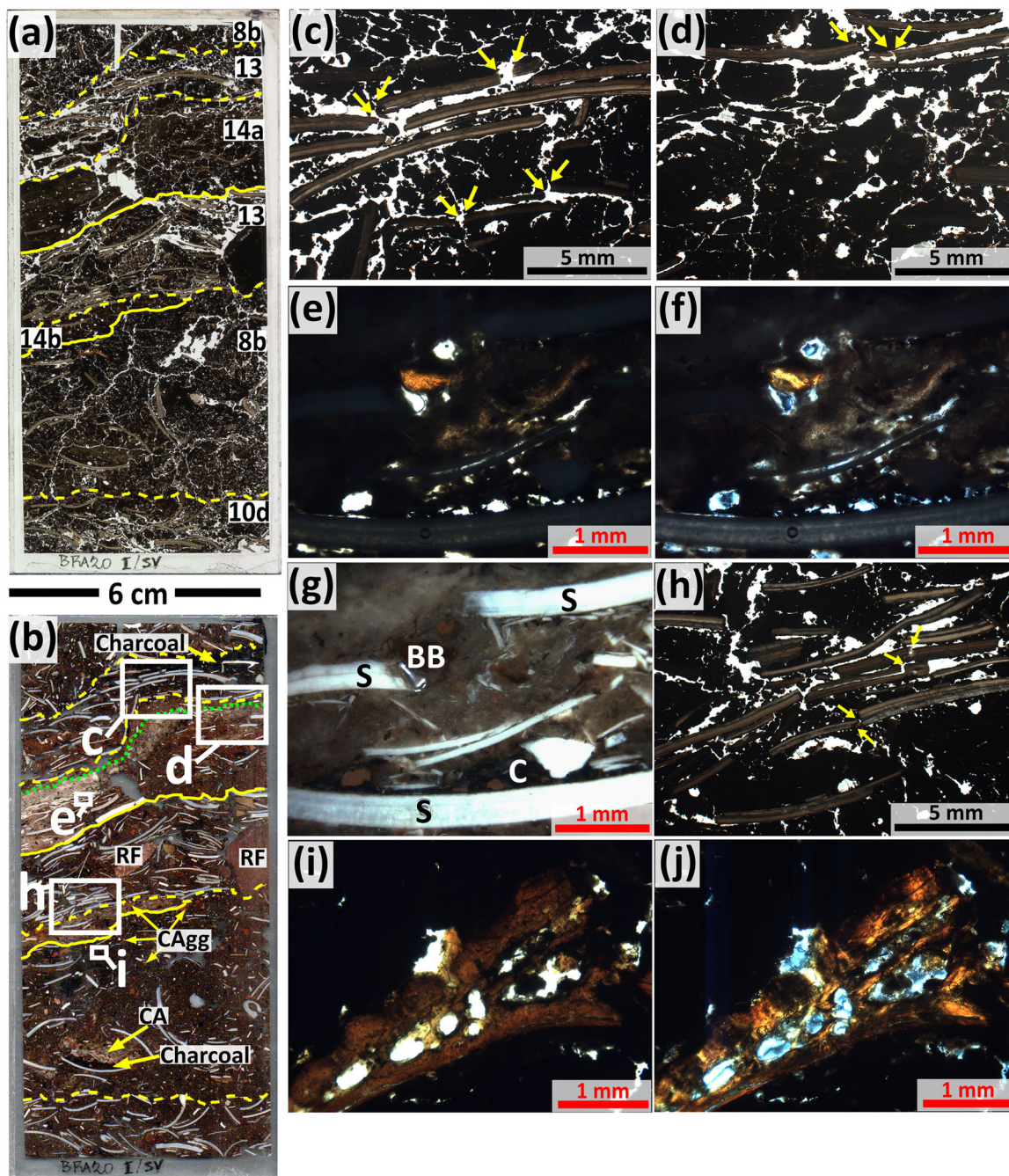


FIGURE 7 | Micromorphology sample I, collected in Sector V. (a) Thin section PPL scan, with microfacies types (8b, 13, 14a, 14b, and 10d) and contacts identified. (b) Dark-field thin section scan, in which shell fragments and other components, such as rock fragments (RF), charcoal, cemented ashes (CA), and clay aggregates (Cagg), are more noticeable. The dotted green line marks the lower contact of an iron-impregnated surface on top of the ash and shell-rich lens mF type 14a. Sectors where photomicrographs were taken are also shown. (c) Photomicrograph of subhorizontal bands of shell fragments in mF type 13, in PPL. Yellow arrows indicate fragments that remain interconnected. Note the dark, highly organic character of the micromass, with highly degraded charcoal on top. (d) View of the contact of mF types 14a (base) and 13 (top) in PPL. Apart from the interconnected shell fragments, note the presence of plates immediately underneath them. (e) Detail of mF type 14a, in PPL. (f) Same as (e), but in XPL, in which the micritic nature of the micromass, as well as shell fragments and a burnt bone, are more visible. (g) Same as (e) and (f), but in OIL, which allows for the observation of all the constituents, including shells (S), a burnt bone (BB), and charcoal (C). (h) Interconnected shell fragments (yellow arrows) from the lower exposure of mF type 13, in PPL. (i) Bone fragment in mF type 8b, in PPL. (j) Same as (i), but in XPL. Birefringence colors probably point toward burning at ~400°C (Villagran, Huisman, et al. 2017). OIL, oblique incident light, PPL, plane-polarized light; XPL, cross-polarized light.

clayey loam layers that gradationally underlie them in Squares 120/107 (Figure 3c,d) and Square V (Figure 4c,d). Distinct “ashy” pinkish gray mottles were observed in F1a in the north section of Square 120/109, possibly related to

recent fire activity at the rock-shelter already noticed by Collet (1978a, p. 5). These top and middle layers, visible in the sectors which are more exposed to weathering, exhibit soil A horizon characteristics.

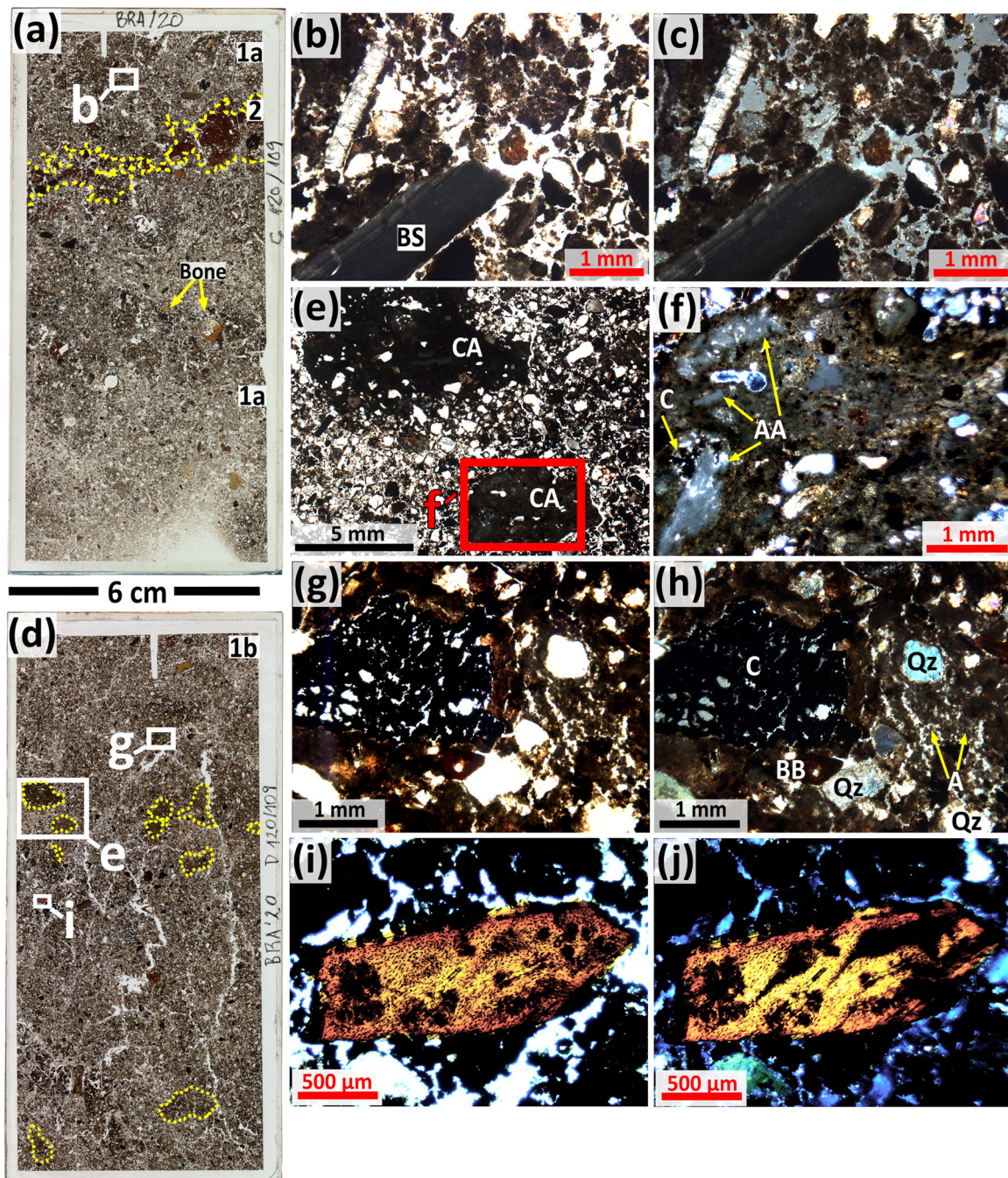


FIGURE 8 | Micromorphology samples C and D, collected in Square 120/109. (a) Thin section scan of sample C, in PPL, indicating microfacies types (1a and 2), sectors where photomicrographs were taken, and bones. (b) Photomicrograph of mF type 1a, in PPL, highlighting unheated (S) and burnt (BS) shell fragments. (c) Same as (b), but in XPL, note micritic crumbs in the micromass. (d) Thin section scan of sample D, in PPL, indicating microfacies type 1b, sectors where photomicrographs were taken, and discrete aggregates of ash pseudomorphs (yellow dotted lines). (e) Photomicrograph of inset rectangle (e) in thin section scan (d) indicating subrounded aggregates of cemented ashes (CA), in PPL. (f) Detail of aggregate of cemented ashes in rectangle (f) in photomicrograph (e), in XPL. Note articulated ashes (AA), charcoal (C), and presence of clay alongside micrite. (g) Photomicrograph of rectangle (g) in thin section scan (d). (h) Same as (g), but in XPL, in which charcoal (C), quartz grains (Qz), and a burnt bone (BB) are indicated. Note ash pseudomorphs (A), secondary micrite, and clay in the micromass. (i) Burnt bone fragment, in PPL, note reddish brown color. (j) Same as (i), but in XPL. PPL, plane-polarized light; XPL, cross-polarized light.

A micromorphological characterization of these layers was made in a thin section prepared from block A (Figure 5a), collected at the base of F5 and top of F6. Under the microscope, this section exhibits a characteristic excremental fabric rich in amorphous organic matter, with a complex

spongy and micro-aggregated microstructure (mF type 7a) that becomes more granular as the sequence grades up (mF type 6) (Figure 5d,e). Faunal channels, passage features, and chambers are observed, these being frequently infilled by fecal pellets of different shapes (Figure 5a). Shell fragments

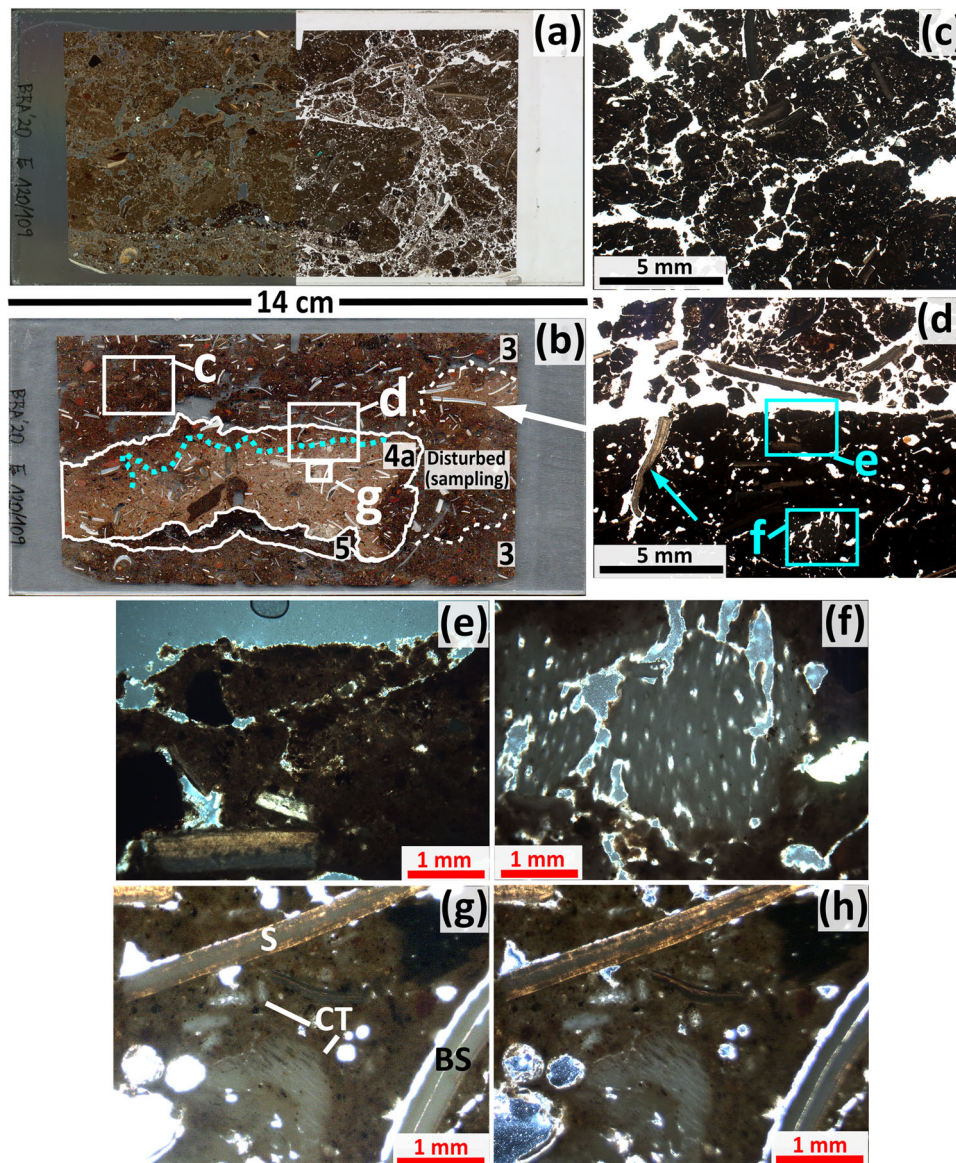


FIGURE 9 | Micromorphology sample E, collected in square 120/109. (a) Thin section scan in PPL (right half) and XPL (left half). (b) Dark-field thin section scan, in which the cemented ash lens mF type 4a and other types (3 and 5) are more visible. Apart from sectors where photomicrographs were taken, a dark iron-impregnated surface on top of the lens is indicated by a turquoise dotted line. (c) Photomicrograph, in PPL, showing porous subangular blocks and crumbs that characterize mf Type 3. (d) Detail of the jagged top of the ash lens, in PPL, indicating a shell fragment filling a void perpendicular to the surface (turquoise arrow). (e) Detail of inset (e) in photomicrograph (d), in XPL, showing plates and a dense micritic micromass. (f) Detail of articulated ashes in inset (f) in photomicrograph (d), in XPL, which exhibit partial dissolution. (g) Detail of inset (g) in thin section scan (b), in PPL, showing partially carbonized tissues (CT), and an unheated (S) and burnt (BS) shell fragment. Also note the presence of vughs. (h) Same as (g), but in XPL. PPL, plane-polarized light; XPL, cross-polarized light.

(Figure 5e) and bones are here the least abundant of all the analyzed thin sections.

3.2 | Particle Size and Initial Parameters

Particle size analysis of the Maximiano Rockshelter deposits revealed overall very different scenarios for the less and more exposed areas. Distributions in samples collected in Square 120/109 exhibit a predominant trimodal pattern, with peaks in the clay, medium/coarse silt, and medium sand fractions, while the ones obtained in Square 120/107 are mostly unimodal either in the very fine sand or fine sand fractions (Figure 11a). Samples

are very poorly sorted in 120/109 ($N = 12$, median = 2.10 phi) and poorly sorted in 120/107 ($N = 15$, median = 1.83 phi), these slight differences being statistically significant (Wilcoxon rank-sum $W = 7$, $p < 0.005$).

Fine-grained fractions are more common in 120/109 ($N = 12$, range from 24.18% to 57.46%) than in 120/107 ($N = 15$, 8.93% to 49.69%) (Wilcoxon rank-sum $W = 41$, $p = 0.02$). Peaks of these size fractions occur in F2a, from 80 cm downward in the F2a-F4 transition, and in both F5 and the shell-rich F7 (Figure 11b). Within the sand-sized fractions, a rather more uniform behavior was found in 120/109, while expressive peaks in 120/107 were seen within the coarser fractions in F6 (with a maximum of 52.15%–55.97% between 50 and

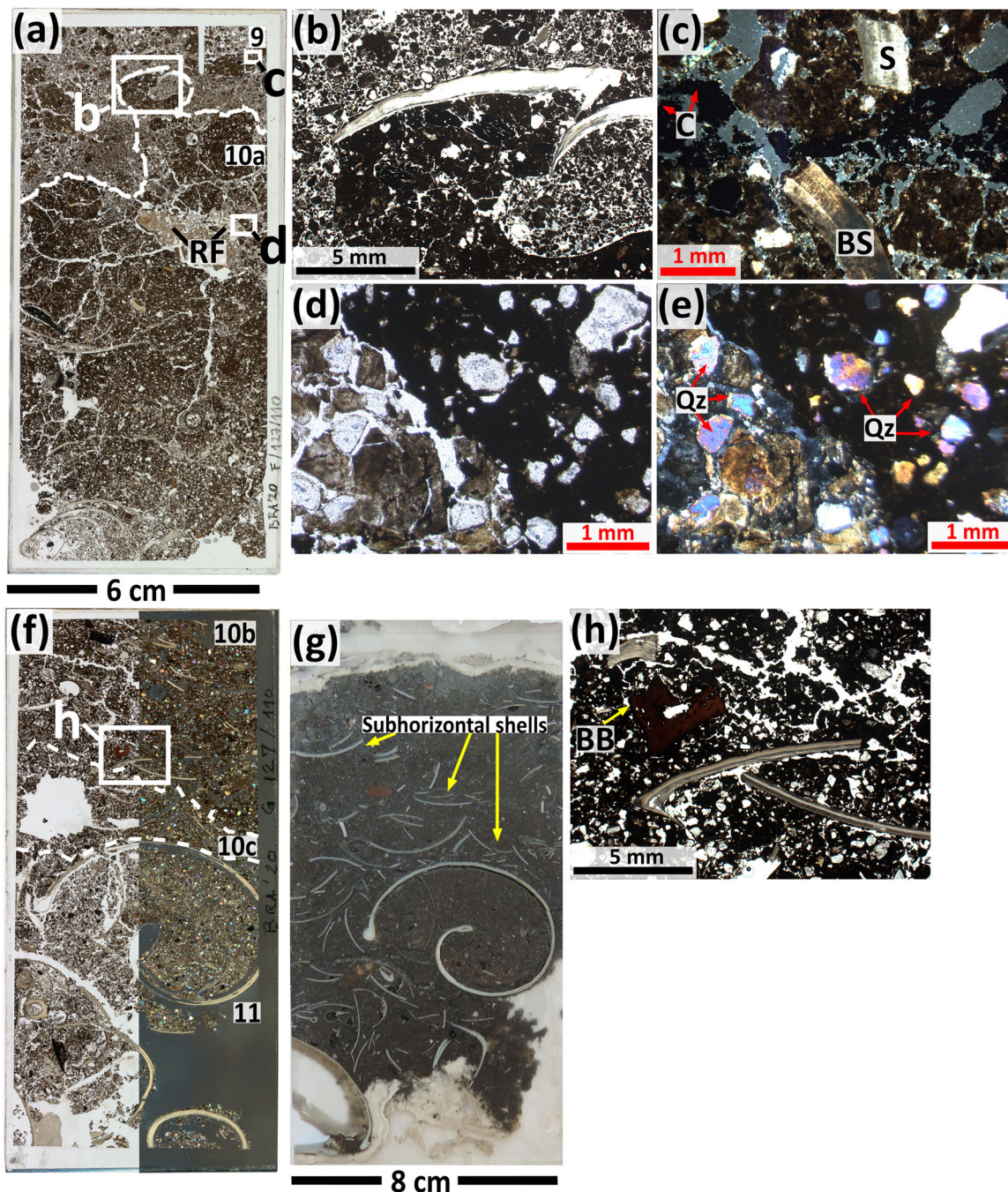


FIGURE 10 | Micromorphology samples F and G, collected in Square 127/110. (a) Thin section scan of sample F in PPL, showing two microfacies types (9 and 10a) and sectors where photomicrographs were taken. Note rock fragment (RF). (b) Photomicrograph of the clear contact of mF types 10a and 9, in PPL, showing a looser, granular matrix in the latter. (c) Example of unheated (S) and burnt shell fragment (BS), and charcoal (C) that are part of the materials of mF type 9, in XPL. (d) Detail of rectangle (d) in thin section scan (a) showing transition between rock fragment and surrounding matrix. (e) Same as (d), but in XPL. Apart from the carbonate nature of the rock, note similar shape and surface aspect between quartz grains (Qz) inside and outside the fragment. (f) Thin section scan of sample G in PPL (left half) and XPL (right half), highlighting microfacies types (10b, 10c, and 11) and sectors where photomicrographs were taken. (g) Photo of impregnated block of sample G, where the complete *Megalobulimus* sp. shell and subhorizontally distributed shell fragments are more visible. (h) Detail of rectangle (h) in thin section scan (f) in PPL, showing a burnt bone (BB). PPL, plane-polarized light; XPL, cross-polarized light.

70 cm deep), and both among the finer and coarser fractions in F7 (Figure 11b). The off-site control sample shows a medium sand mode, being more similar to 120/107's F6 and F8 (Figure 11a), thus suggesting a possible shared origin for the terrigenous fraction of these different contexts.

Values of pH exhibited little variation, oscillating between 7.5 and 8.2 for the one measured in water and between 7 and 7.8 for the KCl method. The minima were found both in basal layers F8 and F16, while maxima were observed in several samples from 120/109, in F2a, F2b, F3, and the F3/F2b transition (Figure 11b).

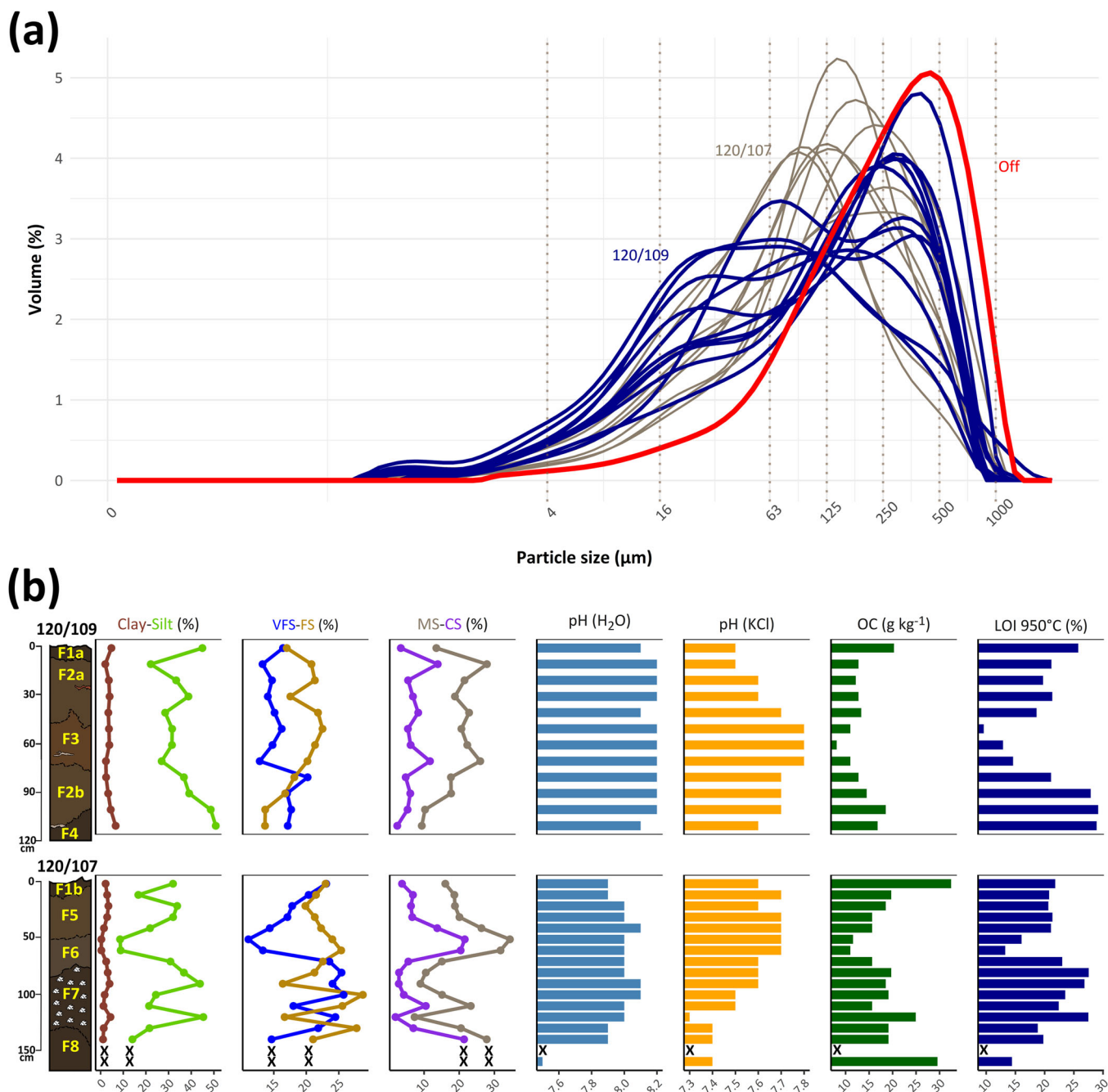


FIGURE 11 | (a) Particle size distributions for facies' bulk samples (without facies transitions) collected in squares 120/109 (blue) and 120/107 (grayish brown), and the off-site control sample (red). Dotted lines indicate limits of major granulometric intervals ($< 4 \mu\text{m}$: clay, $4-16 \mu\text{m}$: very fine silt, $16-63 \mu\text{m}$: medium-coarse silt, $63-125 \mu\text{m}$: very fine sand, $125-250 \mu\text{m}$: fine sand, $250-500 \mu\text{m}$: medium sand, $500-1000 \mu\text{m}$: coarse sand). (b) Stratigraphic comparison of several parameters measured in bulk samples collected in squares 120/109 (top) and 120/107 (bottom). The "X" symbol indicates absence of sample. CS, coarse sand; FS, fine sand; LOI 950°C, loss on ignition at 950°C; MS, medium sand; OC, organic carbon; VFS, very fine sand.

OC values (mean = 17.49 g kg^{-1}) ranged from 8.11 g kg^{-1} in F3 to 32.46 g kg^{-1} in F1b. Facies identified in Square 120/107 ($N=16$, median = 18.84 g kg^{-1}) are overall more enriched when compared to the ones in Square 120/109 ($N=12$, median = 12.75 g kg^{-1}) (Wilcoxon rank-sum $W=153$, $p=0.008$). A depth-coherent decrease in OC is observed in 120/107 up until $\sim 50-60 \text{ cm}$, in F6, this also being the depth around which the lower concentrations were obtained for both squares (Figure 11b, see Supporting Information S1: Table S6). From this depth downward, values increase in both areas, with

sharper peaks in F7 and F8. The values obtained for both the excavated samples from F16 in Square 114/111 ($N=3$, mean: 24.08 g kg^{-1}) and the off-site sample (22.03 g kg^{-1}) were among the ones observed in the upper layers, except for the more enriched F1b.

LOI 950°C values, used in this work as a proxy for carbonates, were similar among the squares compared (median = 21.14% [120/109] vs. 21.22% [120/107], Wilcoxon rank-sum $W=98$, $p=0.94$). Stratigraphically (Figure 11b), this indicator behaved in 120/109 in a

3.3 | Major Elements and INAA

In this section, the results of major chemical elements obtained by both XRF and by the analysis of av. P and extractable cations, as well as of some major, minor, and trace elements derived from INAA, are presented. Element concentrations are provided in full in Supporting Information S1: Tables S7, S8, S10, and S11.

A PCA (Figure 12a) was performed of the data for major elements obtained in the set of samples collected only within each facies (i.e., leaving aside facies transitions) in squares 120/109 ($N = 10$), 120/107 ($N = 12$), and 114/111 ($N = 3$), and in the control off-site sample. The first two principal components (PC) explain together 70.4% of the total variance (see contributions of variables in Supporting Information S1: Table S9). In PC1, the control sample, highly enriched in metals TiO_2 and Al_2O_3 , and in av. P, as well as samples from facies which are enhanced in silica (F2a, F3, and F6), are clearly separated from Ca-rich and P-rich facies (F4 and F7). PC2 basically distinguishes extractable Ca and Mg forms (particularly high in F16) from the silica-rich facies. The analysis seems to differentiate, on the one hand, the effects of terrigenous enrichment (quartz and clay minerals) and, on the other hand, contributions from anthropogenic sources such as mollusk shells and ashes, which are enhanced in carbonates and Mg (Etiégni and Campbell 1991; Karkanis 2021; Middleton and Price 1996; Milek and Roberts 2013) and were observed in thin section. The strong association of CaO with P_2O_5 ($N = 30$, $R^2 = 0.85$, $p < 0.001$) also points at the influence of apatite within these facies.

An HCA was carried out of the log base 10-transformed INAA elemental concentrations obtained for the same batch studied through major element analyses, the exception being for samples now included which yielded below detection limit values in the aforementioned procedures ($N = 2$), and of two others collected in the lenticular cemented ash (mF type 4a) and clay layers (mF type 2) in Square 120/109 (sample details in Supporting Information S1: Table S10). The resulting dendrogram (Figure 12b) allowed for the identification of three clusters. Cluster 1 includes 11 samples, most of them from facies of Square 120/107, with also one from the top of F3, the off-site soil and the clay lens. In cluster 2 ($N = 8$), alongside facies from top (F1a/F2a) and bottom (F4) of Square 120/109, including the ash lens, are grouped together samples from the upper and lower contact of F7. Cluster 3 ($N = 10$) shows a mixture of middle deposits of 120/109 (F2a, F3, and F2b), upper (F1b) and middle (F5) deposits of 120/107, as well as the three F16 samples. While cluster 1 is the most enriched in all the elements, cluster 2 is the most depleted, cluster 3 showing an intermediate position (Supporting Information S1: Table S12). When these clusters were subjected to LDA, the two first plotted discriminant functions showed their clear separation under a 95% confidence interval, despite the presence of possible outliers, the most notable of all being the control sample (Figure 12c).

These three INAA groups seem to distinguish between a sand- and clay-rich scenario encountered in the most exposed area and in specific layers from under the overhang, an ash-rich one

seen mainly in the inner area, and an intermediate organic-rich one composed by dark silt loamy deposits.

3.4 | FTIR Spectroscopy

Minerals detected in nine samples through FTIR spectroscopy are presented in Supporting Information S1: Table S13, alongside the indicative absorbance bands and references used for interpretation. A first glimpse at Figure 13, which compares spectra collected in facies from squares 120/109, 120/107, and the off-site sample, shows an overall similarity between the first two and the great difference with respect to the latter.

Calcite is the main mineralogical constituent of the studied deposits, as indicated by the characteristic carbonate ~ 1421 (ν_3), 874 (ν_2), and 713 (ν_4) cm^{-1} peaks (Chukanov 2014; White 1974). It is present in all the site's samples, not being found in the off-site one. The second major component consists of clay minerals, with the absorbance bands in the hydroxyl (OH) stretching region at ~ 3695 and ~ 3620 cm^{-1} , a singular peak at ~ 1030 cm^{-1} , as well as peaks at around 530, 470, and 422 cm^{-1} , pointing at the possible presence of smectites (Madejová 2003). Clay minerals are slightly more abundant in F6 and F8. Comparison of a sample of the clay lens (mF type 2) with the control sample indicated the same mineralogy (Supporting Information S1: Table S13).

Clear indication of heat-altered clay minerals is lacking, the main Si–O absorption at ~ 1030 – 1035 cm^{-1} not being positioned to higher wavenumbers in any case, as would be expected for heat exposure temperatures equal to or greater than $\sim 500^\circ\text{C}$ (Berna et al. 2007). However, some evidence for clay heating could be present in Square 120/109, such as the absence of the OH absorption bands (in F1a, F2b, and F4) and the smoother aspect (in F4) or disappearance (in F1a) of the absorbance ~ 530 cm^{-1} . Therefore, the mixing of heated and unheated clay minerals in these facies cannot be ruled out. In fact, recent research suggests only a small amount of added unheated clay (up to 10%) is enough to alter spectra from heated sediments (Ogloblin Ramirez et al. 2023).

Minor constituents include quartz and carbonate hydroxyapatite. The former, indicated by the 798 – 778 cm^{-1} Si–O stretching duplet and a peak at ~ 694 cm^{-1} , is more abundant in facies from Square 120/107, with higher peaks in F6 and F8, as well as in the control sample (Figure 13). The latter was detected through the 604 – 565 cm^{-1} duplet (Figure 13) in all facies but F1b, F6, F8, and off the site.

4 | Discussion

The Maximiano Rockshelter deposits are the product of a complex suite of processes taking place in a highly dynamic tropical Atlantic rainforest environment. Micromorphology and other geoarchaeological techniques have shown the interplay of human activities and geogenic processes that characterize this site. These are now discussed in detail, together with the different post-depositional pathways by which they have been affected.

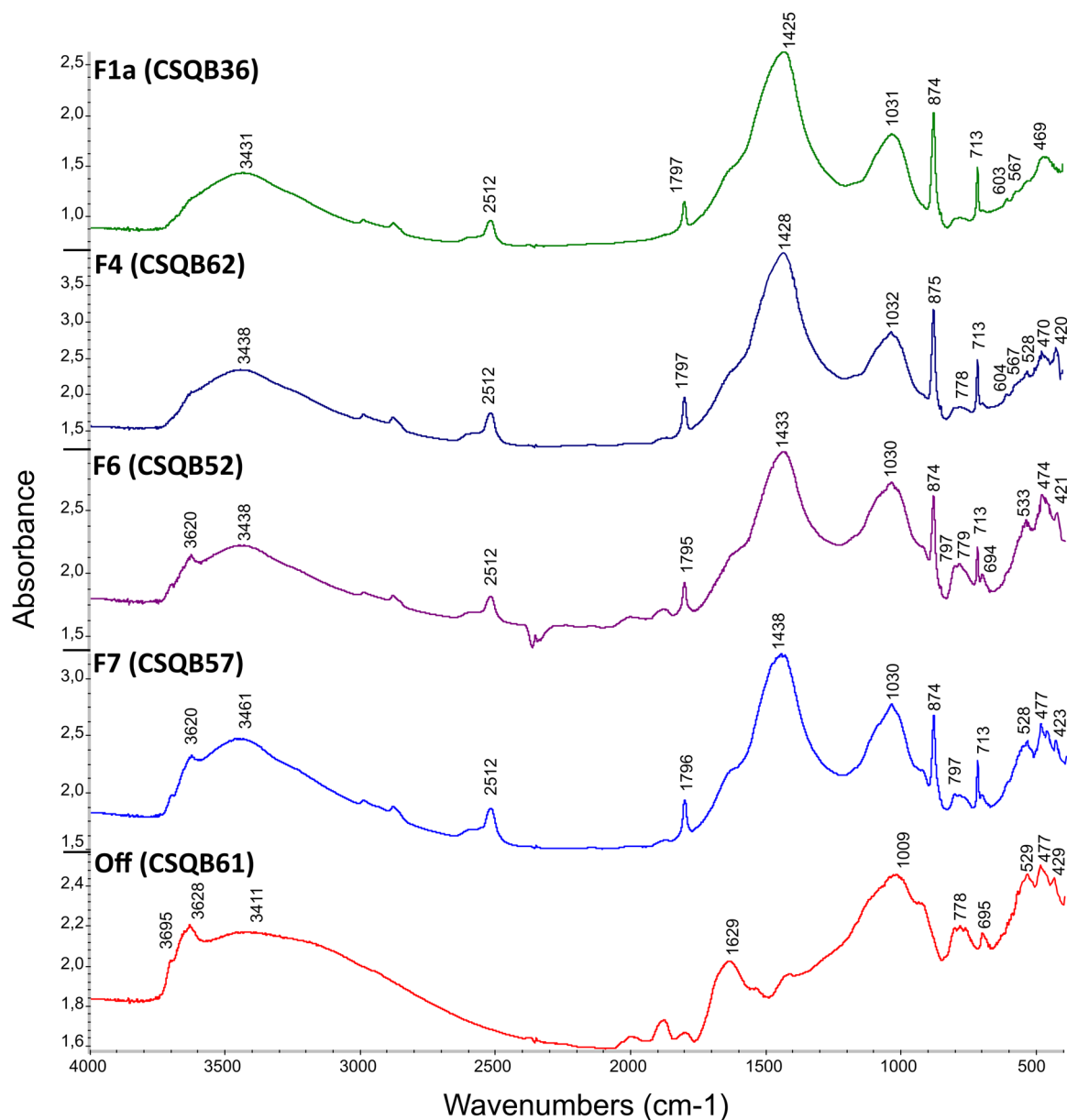


FIGURE 13 | Representative FTIR spectra of facies identified in Square 120/109 (F1a and F4), Square 120/107 (F6 and F7), and in the off-site control sample (Off). Calcite (2512, 1795–1797, 1425–1438, 874–875, 713 cm^{-1}) is the main component of the shelter's sediment, not being detected outside the shelter. Clay (3620, 3431–3438, 1030–1032, 528–533, 469–477 cm^{-1}) is the second major component of the site, more abundant in F6 and F7, and the dominant material in the control sample. Traces of carbonate hydroxyapatite (small duplet 604 and 567 cm^{-1}) are visible in F1a and F4. Quartz (797, 778–779, 694–695 cm^{-1}) is present in small amounts in F4, increasing in F6, F7, and the off-site soil.

4.1 | Dumping/Tossing of Shells and Other Materials, and the Construction of Bedded Sequences

The shell fragment-rich deposits with gravel-sized bones, lithic artifacts, and charcoal, encountered in F7 and part of F15, microscopically characterized in mF types 8a and 8b, represent the poorly sorted chaotic anthropogenic mix of occupation-derived materials encountered in several shell-matrix sites from around the world (Aldeias and Bicho 2016; Grono et al. 2022; Villagran 2019). Massive accumulations of debris with different trajectories have been globally interpreted as evidence of deliberate midden formation (Matthews et al. 1997; Needham and Spence 1997; Shillito and Matthews 2013). Micromorphology work undertaken by Villagran

(2014, 2019) and colleagues (Villagran et al. 2009) in the coastal shell mounds of Brazil interpreted similar microfacies (mF type A) as reworked deposits resulting from activities like basket-load dumping of refuse, mostly composed by shell fragments, which were previously discarded at other locations. The presence, in mF type 8a, of bones heated to various temperature ranges, together with unburnt bones and other materials, suggest they were part of different activity contexts before final deposition. Anthropogenic mixing is also indicated by the absence of the characteristic stratigraphic sequence of primary combustion structures (e.g., reddened substrate, charcoal and ash (see Mentzer 2014; Mallol et al. 2017), the presence of loose ash/reprecipitated ash aggregates throughout the groundmass, as well as by areas of shell fragments (some of them interconnected, e.g., Figure 5c,h) with associated

reprecipitated ashes. The organic-rich character of the micromass, also indicated by high OC values of F7, makes these mF types similar to the ones found in shell-bearing deposits in Portugal (Cabeço de Amoreira's mF type 4, Aldeias and Bicho 2016) and Vietnam (Thach Lac's mF A, Grono et al. 2022).

Subhorizontally distributed gastropod shells, seen in F10, F11, F14, and at the base of the stratified sequence F15, characterized in mF types 10a-d and 11, can be interpreted as the product of tossing. Characterized in thin section through this predominant distribution pattern of shell fragments, oriented in lines and/or bands, discrete events of shell tossing are considered to represent the immediate discard of shells and other remains which were slightly disturbed over time (Aldeias and Bicho 2016; Duarte et al. 2019; Villagran 2019; Villagran et al. 2011). In Maximiano, the sequence from mF type 11 to 10a, in thin-sections G to F, exhibit shell fragments in between complete specimens, as well as fragments that are increasingly reworked going upward. The fact that closely packed complete specimens exhibit a linear orientation (Figures 4b,d) points also toward the deliberate arrangement of gastropod shells. Anthropogenic layers/lenses mainly composed of either subhorizontal complete snail shells or snail shell fragments have been identified elsewhere (e.g., Rabett et al. 2011), with still few micromorphological examples (e.g., Linstädter and Kehl 2012; Lombardo et al. 2013).

Shell-rich laminae that make part of the stratified sequence seen in F15 also exhibit fragments in a sub-horizontal/horizontal distribution (mF type 13), but these differ with the ones in the aforementioned mF types, both in a closer association with frequent charred materials and in the evidence of in situ fragmentation for most of them. While these layers could be the result of tossing episodes as well, the fact that the shells are closely packed, slightly vertically displaced, and interconnected suggests the presence of trampled surfaces, another recurrent syn/post-depositional characteristic inferred in shell-bearing sites (Aldeias and Bicho 2016; Balbo et al. 2010; Duarte et al. 2019; McAdams et al. 2022; Morrissey et al. 2023; Villagran 2019; Wurz et al. 2022; Zerboni 2011). Even when other processes applying compression over shell-rich surfaces cannot be ruled out, the microstructure of angular blocky peds and plates separated by planes, which is visible immediately below the shells, is also a common micromorphological indication of trampling (e.g., Araujo et al. 2008; Gé et al. 1993; Matthews et al. 1997; Milek and French 2007; Milek 2012; Rentzel et al. 2017; Shilito and Ryan 2013).

The stratigraphic succession of F15 shows a clear pattern of specific anthropogenic inputs that intercalate each other, the ash- and shell-rich (mF types 14a-b) laminae/layers being underneath the sub-horizontal/horizontal shell- and charcoal-rich ones (mF type 13). The intimate association of mostly unheated linear shell fragments and charcoal has been reported for shell mounds with a sandy core on the Brazilian coast (mF type F of Villagran 2019).

4.2 | Fire-Related Activities, Structures, and Reworking

The main indicator for the presence of fire at the microscopic level among Maximiano's deposits consists of ash pseudomorphs, which are produced after the complete combustion of plant matter

(Braadbaart and Poole 2008; Braadbaart et al. 2012; Canti 2003; Canti and Brochier 2017; Mentzer 2014). Single ash crystals as well as lenticular layers/lenses and subrounded aggregates with both discrete/articulated and reprecipitated ash pseudomorphs forming secondary micrite were observed in thin section.

In the case of the loamy deposits of the central area under the rock ledge (F2a,b, F3, and F4), ashes make up part of a suite of materials exposed to heat as well as of unheated constituents, mostly sand-sized quartz grains and rock fragments. Particle size analysis of their terrigenous fraction showed these deposits to be overall very poorly sorted and rich in clay and silt when compared to the ones in the most exposed area of the shelter. The impact of ashes in these facies is indicated by a common INAA grouping (cluster 2) of some of them with a sample from a cemented ash lens (mF type 4a, see below). This pattern of ash-rich (cluster 2) versus terrigenous-rich (cluster 1) clustering of deposits, the first one being more chemically depleted, has previously been found by INAA within the karstic Taquaraçu Rockshelter of southeastern Brazil (Tudela et al. 2020).

Heterogeneous mixed deposits (mF types 1a,b) of the kind found in this area, with frequent burnt materials, are a common presence in rock-shelter and cave settings (Araujo et al. 2008; Araujo and Piló 2017; Goldberg et al. 2009; Marcuzzan et al. 2022; Miller et al. 2013; Schiegl et al. 1996; Silva 2022; Villagran, Strauss, et al. 2017). Experimentally based interpretation of poorly sorted, rounded ash aggregate-rich accumulations (Mallol et al. 2013; Miller et al. 2010) suggest they are formed by dumping materials away from where combustion is taking place. They would, in such a case, represent the product of site maintenance activities (Schiffer 1987). Differentiating dumping from sweeping of combustion materials can be difficult, however (Miller et al. 2010).

Observations made by Collet suggest the origin of at least part of the materials found within these mixtures could be in the northwest sector of Square 120/109, excavated in 1978. He claimed to have observed, in that sector, "20 hearth layers" (Collet 1978b, p. 18) between 1 and 6 cm thick, up to a depth of 120–130 cm. As the north profile is nowadays partially collapsed, sampling was not possible. Had hearths been present in this part of the site, they could explain the metric accumulations of combustion-derived and other residues that occur in Square 120/109. Activities like sweeping, rake-out, dumping, and trampling could have then reworked these materials further down to the south, where they were observed in thin section. Future excavation and micromorphological analyses will help address this issue.

The lenses of cemented ashes (mF type 4a) that are encountered throughout the loamy facies of the inner part of the site are a recurrent anthropogenic deposit in archaeological karstic caves (Courty et al. 1989; García et al. 2024; Shahack-Gross et al. 2008). The fact that cementation, by forming a crust resistant to erosion, contributes for ash preservation (Karkanas 2021; Mentzer 2014; Shahack-Gross et al. 2014) is indicated by several domains of articulated ashes amid mostly massive and vughy secondary micrite-rich lenses and aggregates (Figures 8f and 9g,h). The charcoal layer/lens (mF type 5) that is sharply bounded underneath mF type 4a could indicate that the sequence is part of a primary combustion structure. However, the highly separated character of the stacked lenses from the surrounding organic

blocky matrix (mF type 3) suggests they are not in primary position. Moreover, the Fe-impregnated top of the ash lens indicates exposure of this surface to wetting/drying cycles or to temporal retention of moisture (Gé et al. 1993; McAdams et al. 2022; Miller et al. 2013) prior to deposition in this part of the site. This surface was also likely impacted by trampling, as suggested by its jagged aspect with voids, some infilled by shell fragments, by its platy aspect, and subhorizontally distributed shell fragments (Araujo et al. 2008; Banerjea et al. 2015; Milek 2012).

The F13 bedded lenticular sequence in which ash-rich layers (mF type 4b), with well-preserved ash pseudomorphs (some of them articulated), alternate with reddened clay accumulations (mF types 12a and 12c) is indicative of superimposed primary combustion features separated by reworked sediments (Mallol et al. 2017; Mentzer 2014). Undulating laminated ashes and partially carbonized tissues at the base of one of the massive ash lenses (Figure 6f), these in turn being on top of a reddened clay lamina (mF type 12b), further point toward the typical stratigraphic sequence of hearths in this area (Karkanas 2021; Karkanas and Goldberg 2018; Mentzer 2014; Miller et al. 2013; Schiegl et al. 1996; Shahack-Gross et al. 2014). Stacking (superimposing by relighting) hearths over time improves hearth visibility in archaeological contexts (Aldeias 2017; Karkanas 2021; Shahack-Gross et al. 2014), leaving behind, in many cases, only “ashy hearths” or lenses (Mentzer 2014; Villagran, Strauss, et al. 2017). Reworking of ashes and clayey substrates with other burnt materials could have been produced by sweeping and/or hearth rake-out, these being suggested by open granular microstructures (Goldberg et al. 2009; Mallol et al. 2013) and sub-horizontally oriented cm-sized materials like burnt shell fragments (Figure 6b) which are left behind by cleaning lateral movements (Homsey and Capo 2006; Miller et al. 2010; Sisa-López de Pablo et al. 2022).

4.3 | On Sources, Gaps, and Surfaces

Micromorphology revealed that the main source of the site's sand-sized fraction comes from the attrition of the host meta-carbonate rock, as seen in thin section F. The subangular, commonly dotted-altered quartz grains that are seen detaching from rock fragments are more frequent in the eastern area of the rock-shelter (Figure 10d,e). As the rock ledge here is less inclined and more exposed to weathering, a more frequent supply of roofspall is expected. Petrographic studies of meta-carbonate rocks from the same region report similar characteristics to the ones observed in Maximiano, quartz always being the main accessory mineral (Frasca 1993).

The FTIR data indicated that the clay minerals present in the mF type 2 lenses are the same as the ones in the immediate site surroundings. Although a specific study is needed to determine clay mineralogy (e.g., XRD), smectites as here found alongside others have been reported for the young soils present in hilly areas of this sector of the Atlantic Forest (Silva 1985). The clear LOI 950°C, major and multi-element differences separating the site's samples from the control, point toward different geochemical pathways in which the anthropogenic factor is crucial. The combined effect of ashes and bones, the first also indicated by INAA cluster 2, must be

behind the enrichment in CaO and P₂O₅ of F4 and F7, these components being observed in respective mF types.

Evidence for an allochthonous origin of sediment was observed in mF type 14b, where frustules of diatoms and potential phytoliths were found adjacent to clay aggregates (Supporting Information S1: Text S1). While a specific study is needed to tackle this, it is clear that at least part of this sediment was collected at the edge of a body of water (Goldberg et al. 2009).

A pause or gap in anthropogenic deposition could be present in squares 120/109 and 120/107. The gradual depletion of humic material and clay from mF type 8a (base) toward mF type 7b (top), with sand-size grains becoming mostly bridged by these and closely packed (see details in Supporting Information S1: Figure S3), could indicate the succession of pedogenesis (affecting F7) and washing out of the micromass in a surface exposed to rainfall (Williams et al. 2018). Bioturbation affected part of mF type 1b (see Figure 8d and Section 4.4) at roughly the same depth in 120/109. The loss of fine material is also indicated by the presence of peaks in coarse grain-size fractions between 50 and 70 cm depth in Square 120/107, the lowest values of OC and LOI 950°C at around the same depth for both sampled columns (Figure 11b), as well as by the silica-rich character of F6 and part of F3 as seen through major elements and FTIR. Considering the difference between standard deviations of calibrated radiocarbon ages for F7 and the base of F2a (see Table 1 and Figure 3a,c), this gap represents at least 1058 years. Possible paleoenvironmental implications of this potential gap are discussed in Section 4.5.

Apart from the trampled occupation surfaces seen within the F15 sequence, other surfaces or paleo-surfaces could be present. The sudden peak in OC, as well as the similarity, with the off-site sample, in grain-size distribution of the basal organic very dark brown deposit F8 in Square 120/107 could point toward a buried soil A horizon (French 2022). However, the fact that this layer is underneath F7 could also indicate OC enrichment by downward migration. This could potentially explain the young age for this deposit of ca. 1310 B.P. (Beta 432546) by contamination. More dating as well as micromorphology work is needed to tackle this problem.

4.4 | Post-Depositional Processes

Overall, the Maximiano deposits exhibit good preservation conditions for organic remains. This is not only indicated by the presence of bones, mollusk shells, and ash pseudomorphs but also by pH values (> 7.3 in most samples) which are characteristic of stable conditions for them (Berna et al. 2004; Karkanas 2010; Karkanas et al. 2000, 2002; Weiner 2010). As calcite is the major mineral making up these sediments (indicated by FTIR spectroscopy), its capacity of buffering the pH of water would prevent alteration of those materials (Weiner 2010).

Micromorphological analysis revealed that bioturbation played a major role in altering the site's deposits. Features related to mesofauna are most conspicuously seen in the organic-rich microfacies (mF types 6, 7a-b), typical of a soil A horizon, in the

more exposed Square 120/107, as inferred by spheres, spheroids, and mamillated excrements (Bullock et al. 1985, p. 133–136; Kooistra and Pulleman 2018; Ismail-Meyer et al. 2018). These constitute coalesced microaggregated microstructures but also infillings within chambers and channels. Modification of pre-existing voids by fauna could be behind the rough planes seen in mF type 1b (Kooistra and Pulleman 2018). Extensive humification is also indicated by the higher OC values obtained for the upper and medium facies, which coherently diminish with depth until ~50 cm. A similar process is likely occurring in the top and middle deposits of Sector V, also located in an area which is more exposed to weathering. Strong humification is also visible in the stratified sequence F15 at ~60 cm from the surface in Sector V.

The site is also being affected by macrofauna, as observed in a *tatu* (armadillo) burrow at the base of Square 120/109. These animals have a great impact on the archaeological record (Araujo and Marcelino 2003). Moreover, the agency of insects like leaf-cutting ants (genus *Atta*), which have a strong impact on soil macro and microstructure in the Neotropics, cannot be ruled out. In fact, the porous microgranular aspect of mF types 6 (Figure 5a) and 9 (Figure 10a,b), with subangular aggregates detached from the underlying layers, is characteristic of the intense reworking these ants can produce in tropical soils (Nascimento et al. 2024).

Apart from trampling and the reworking of combustion features and shell-bearing facies-derived materials, humans must also have had another important role in affecting the site's deposits by burying their dead. Future excavation and geoarchaeological analyses should take this into account, as this activity can have a great impact on the sediments (Burns et al. 2017).

Moisture and seasonal rains are another major agent affecting archaeological soils and sediments in tropical rainforest environments, even in cave entrances and rock-shelters (e.g., Kourampas et al. 2009; McAdams et al. 2020, 2022; Morley 2017; Stephens et al. 2017). In Maximiano, the impact of meteoric and percolating waters was seen in the cementation and recrystallization of ash, as well as in the dissolution giving way to secondary micrite. In the case of the combustion features of F13, the good preservation of ash pseudomorphs, the presence of calcite coatings inside voids, iron nodules (Figure 6d,g), as well as localized microsparitic infillings not completely occluding void space (Figure 6j) point to vadose conditions and to a punctual impact of water infiltration/saturation and downward migration (Flügel 2004, p. 94–95; Mallol and Goldberg 2017; Vepraskas et al. 2018). As already mentioned, wet/drying cycles may have played a role in temporarily exposed surfaces.

4.5 | Occupation History and Its Relationship With the Ribeira de Iguape Riverine *Sambaquis*

From a chronological point of view, occupation at Maximiano roughly coincides with the three periods of shell-matrix site construction identified by Figuti et al. DeBlasis (2013) for the Ribeira de Iguape basin: (1) Period 1, which was centered around the Cajati area, involves the first components of the Capelinha I and Batatal I sites (see Figure 1c), dating back to between 9250 ± 50 and

8500 ± 70 year B.P. (10,375 and 9473 median cal years B.P.); (2) Period 2, with sites all across the basin (see Figure 1c), is the most extensive, ranging from 6980 ± 90 to 3530 ± 70 year B.P. (7779–3767 median cal years B.P.); (3) Period 3, centered around the more inland, western area, which dates back to between 1730 ± 40 and 1219 ± 24 year B. P. (1595–1086 median cal years B.P.). The first, early Holocene period fits between the conventional age obtained by Collet and the one here reported for the F7-assigned deposit. The second, mostly mid-Holocene period is contemporaneous with the main occupation at Maximiano, involving both the reworking of combustion features and tossing of complete shells and fragments at Square 127/110 (F13/F12 transition, and F11), and the accumulation of organic and combustion-derived debris at Square 120/109 (from F16 up to the uppermost F2a-assigned deposit). Finally, the last, late Holocene period, coincides with the date obtained for the human metatarsal (Table 1).

Human occupation at the site would have begun immediately after the Younger Dryas (ca. 12,870–11,700 cal year B.P., after Cheng et al. 2020), which in southeastern Brazil was characterized by high precipitation in speleothem records (Cruz et al. 2006; Deininger et al. 2019). The construction of F7, as well as the initial occupation of the riverine and coastal *sambaquis* (Cambriu Grande site, see Calippo 2004 and Figure 1c), would have taken place under drier, hotter, and forested early Holocene conditions for this wider region (Cruz et al. 2006; De Oliveira et al. 2014; Ledru et al. 2015; Pessenda et al. 2009; Saia et al. 2008). The potential depositional gap encountered in Squares 120/109 and 120/107 is coincidental with a scenario of climatic instability in southern and southeastern Brazil between 8 and 8.5 ka cal years B.P. (Bernal et al. 2016; Sallun et al. 2012). Finally, conditions more humid than the early Holocene (Cruz et al. 2006), with sea level rise in nearby coastal areas (Sallun et al. 2012), would have been present during the main occupation of the site.

While the comparison of specific artifactual classes and technologies between the rock-shelter and the riverine *sambaqui* is outside the scope of this work, a macroscopic stratigraphic resemblance of some deposits is noticeable. The presence of *Megalobulimus* spp. shell-rich dumps like the one here described as F7, with frequent lithic and faunal remains and a dark organic matrix, of thicknesses ranging from 10 cm to a meter, has been reported for sites in different sectors of the basin, from the west (Itaóca/Adrianópolis counties) to the east (Miracatu/Pedro de Toledo counties) (Barreto 1988; Collet and Prous 1977; Figuti and Plens 2014; Plens 2009; Tognoli 2016) (see Figure 1c). Lenses of complete shells of land snails, such as the ones observed in F11, but also of bivalves were described for the Moraes, Estreito and Capelinha I *sambaquis* (Figuti and Plens 2014; Penin 2005; Plens 2009) (see sites in Figure 1c). The association of these lenses and dumps with burials, either on top or around them has also been noticed for these sites (Figuti et al. 2013; Tognoli 2016). Moreover, when comparing isotopic data ($\delta^{13}\text{C}$ and $\delta^{15}\text{N}$) obtained from human remains from the Moraes *sambaqui* and soft tissues of *Megalobulimus* spp., Plens (2009) found a negligible, nonintensive contribution of the snails to the diet, suggesting that its collection was mainly driven by building purposes.

The lack of micromorphological studies at these *sambaquis* precludes more systematic comparisons with the results here presented. A study carried out by Teixeira et al. (2012) at the Moraes

sambaqui, which measured grain-size and geochemical parameters (including av. P and interchangeable ions), found an overall chemical enrichment at the site relative to the surrounding natural soil.

Due to its stratigraphic resemblance with these sites, and its characterization as a shell-matrix site with at least one layer with 50% of shell remains (see Andersen 2000 and Villagran 2019) and the presence of characteristic facies and microfacies reported herein, Maximiano can be considered as part of the Ribeira de Iguape riverine *sambaqui* phenomenon. Although in Brazil the term *sambaqui* is commonly used to refer to the decametric multi-stratified monumental shell mounds of the coast (e.g., DeBlasis et al. 2021; Gaspar et al. 2008, 2014; Klokler 2014) and elsewhere (Pugliese et al. 2019), it has also been applied to smaller structures such as the Ribeira de Iguape sites and others (e.g., Villagran et al. 2018). Despite site type attribution (e.g., shell-midden, shell-bearing midden site, see Widmer 2014) of the Maximiano Rock-shelter being beyond the scope of this work, it has been shown that while some facies (F7) were composed of secondary refuse probably coming from different middens or discard areas, in others, shells were used for the construction of surfaces (F15) and layers (e.g., F11) following specific sequences.

5 | Conclusion

In this paper, we offered the first geoenvironmental glimpse of a complex shell-matrix rock-shelter site in the humid Neotropics. The approach has sought not only to distinguish the major geogenic, biogenic, and anthropogenic forces and sources acting within the site but also to identify the types of human activities and behaviors behind depositional patterns. Specifically, this work has shown different deposits of land snail shells of clear human origin. Future systematic excavation coupled with the analysis of macro-artifacts, faunal remains, botanical remains, and other proxies will allow a deeper understanding of these and other activities and processes.

This article has shown that even when archaeological sites in tropical settings are highly affected by a range of processes and agents, a combined micromorphological and geochemical approach can reveal depositional patterns. Despite being covered by a rock ledge, Maximiano has been affected by strong humification in some parts of the site. The impact of bioturbation, rainforest humidity, and seasonal rains, however, has not erased past human activities and features like hearths and their main by-products. Occupation surfaces and deposits are not always completely obliterated by pedogenesis in the humid tropics, even in open air settings (Araujo and Piló 2017; Araujo et al. 2013, 2017).

Author Contributions

Nicolás Batalla: conceptualization, investigation, writing—original draft, methodology, writing—review and editing, visualization, funding acquisition, formal analysis, data curation, software. **Mercedes Okumura:** conceptualization; investigation, funding acquisition, writing—review and editing, validation, resources. **Casimiro S. Munita:** conceptualization, supervision, software, data curation, formal analysis, methodology, validation, writing—review and editing, investigation, funding acquisition, resources. **Charles French:** supervision, writing—

review and editing, methodology, funding acquisition, validation, software. **Astolfo G. M. Araujo:** conceptualization, investigation, funding acquisition, writing—review and editing, methodology, validation, supervision, resources, data curation, project administration.

Acknowledgments

Financial support for this research came from the São Paulo Research Foundation (FAPESP), under grants no. 2023/18132-2, 2018/14293-3 and 2020/04283-0 awarded to Nicolás Batalla, grants no. 2013/13794-5 and 2019/18664-9 to Astolfo G. M. Araujo and grant no. 2018/23282-5 to Mercedes Okumura; the National Council for Scientific and Technological Development (CNPq) (Productivity in Research Fellowship 308856/2022-8), and the PRINT USP CAPES Exchange Visitor Program PVEJS 16/2020 (88887.569895/2020-00), both granted to Mercedes Okumura. The permit to work at Maximiano was granted by the PETAR park authorities and IPHAN (National Institute of Historic and Artistic Heritage). We are also grateful to the following people: Mr. Irineu “Tiço” Ramos, for taking us to the site and assisting with fieldwork activities; Dr. Tonko Rajkovača and Dr. Mike Lewis (University of Cambridge, UK), for respectively helping with the production of the thin sections and FTIR spectroscopy; Prof. Paulo C. F. Giannini (University of São Paulo, Brazil), Prof. Francisco S. B. Ladeira (University of Campinas, Brazil), Prof. Júlio C. Rubin (Pontifical Catholic University—Goiás, Brazil), Prof. Ximena S. Villagran (University of São Paulo, Brazil), Dr. José H. Fontenelle (Santos Metropolitan University, Brazil), and Dr. Diego Terra Machado (University of Campinas, Brazil), for sharing their observations and thoughts on several aspects of this work; Dr. Rogério Bária, Ms Sc Joanna Barros, Dr. Angislaine Costa, and Dr. André Nogueira for helping with laboratory analyses; Dr. David Reich (Harvard University, USA) for the dating of bone sample MAX-48; and the review editor and two anonymous reviewers whose comments greatly helped to improve this work.

Data Availability Statement

The data that supports the findings of this study are available in the supplementary material of this article.

References

- Afonso, M. C. 2019. “Pesquisas arqueológicas no vale do rio Ribeira de Iguape (Sudeste-Sul do Brasil): uma síntese.” *Revista del Museo de La Plata* 4, no. 2: 463–480.
- Aldeias, V. 2017. “Experimental Approaches to Archaeological Fire Features and Their Behavioral Relevance.” *Current Anthropology* 58: 191–205. <https://doi.org/10.1086/691210>.
- Aldeias, V., and N. Bicho. 2016. “Embedded Behavior: Human Activities and the Construction of the Mesolithic Shellmound of Cabeço da Amoreira, Muge, Portugal.” *Geoarchaeology* 31, no. 6: 530–549. <https://doi.org/10.1002/gea.21573>.
- Andersen, S. 2000. “‘Køkkenmøddinger’ (Shell Middens) in Denmark: A Survey.” *Proceedings of the Prehistoric Society* 66: 361–384. <https://doi.org/10.1017/S0079497X00001857>.
- Araujo, A. 2016. *Projeto “A ocupação paleoíndia do Estado de São Paulo: uma abordagem geoarqueológica II”*. FAPESP.
- Araujo, A., J. Feathers, M. Arroyo-Kalin, and M. Tizuka. 2008. “Lapa Das Boleiras Rockshelter: Stratigraphy and Formation Processes at a Paleoamerican Site in Central Brazil.” *Journal of Archaeological Science* 35: 3186–3202. <https://doi.org/10.1016/j.jas.2008.07.007>.
- Araujo, A., J. Paisani, T. Schrage, J. Feathers, G. Hartmann, and O. Ricci. 2017. “The ‘Lagoa do Camargo 1’ Paleoindian Site: Some Implications for Tropical Geomorphology, Pedology, and Paleoenvironments in Southeastern Brazil.” *Geoarchaeology* 32: 662–677. <https://doi.org/10.1002/gea.21628>.
- Araujo, A., and L. Piló. 2017. “Towards the Development of a Tropical Geoarchaeology: Lagoa Santa as an Emblematic Case Study.” In *Archaeological and Paleontological Research in Lagoa Santa: The Quest*

- for the First Americans, edited by P. Da-Gloria, W. Neves, and M. Hubbe, 373–391. Springer International Publishing. https://doi.org/10.1007/978-3-319-57466-0_17.
- Araujo, A., A. Strauss, J. Feathers, J. Paisani, and T. Schrage. 2013. "Paleoindian Open-Air Sites in Tropical Settings: A Case Study in Formation Processes, Dating Methods, and Paleoenvironmental Models in Central Brazil." *Geoarchaeology* 28, no. 3: 195–220. <https://doi.org/10.1002/geoa.21442>.
- Araujo, A. G., and J. C. Marcelino. 2003. "The Role of Armadillos in the Movement of Archaeological Materials: An Experimental Approach." *Geoarchaeology* 18: 433–460. <https://doi.org/10.1002/geoa.10070>.
- Arpin, T., C. Mallol, and P. Goldberg. 2002. "Short Contribution: A New Method of Analyzing and Documenting Micromorphological Thin Sections Using Flatbed Scanners: Applications in Geoarchaeological Studies." *Geoarchaeology* 17, no. 3: 305–313. <https://doi.org/10.1002/geoa.10014>.
- Auler, A. 2019. "Histórico, ocorrência e potencial de cavernas no Brasil." In *Cavernas—Atlas do Brasil subterrâneo*, edited by E. Rubbioli, A. Auler, D. Menin, and R. Brandi, 14–51. Instituto Chico Mendes de Conservação da Biodiversidade.
- Balbo, A., M. Madella, A. Vila, and J. Estévez. 2010. "Micromorphological Perspectives on the Stratigraphical Excavation of Shell Middens: A First Approximation From the Ethnohistorical Site Tunel VII, Tierra del Fuego (Argentina)." *Journal of Archaeological Science* 37, no. 6: 1252–1259. <https://doi.org/10.1016/j.jas.2009.12.026>.
- Banerjee, R., M. Bell, W. Matthews, and A. Brown. 2015. "Applications of Micromorphology to Understanding Activity Areas and Site Formation Processes in Experimental Hut Floors." *Archaeological and Anthropological Sciences* 7, no. 1: 89–112. <https://doi.org/10.1007/s12520-013-0160-5>.
- Barreto, C. 1988. "A ocupação pré-colonial do vale do Ribeira de Iguape, SP: os sítios concheiros do médio curso." Unpublished Master's diss., University of São Paulo.
- Barreto, C., P. DeBlasis, E. Robrahn, C. Dias Neto, I. Karmann, and C. Lino. 1984. "Abismo 'Ponta de flecha': um projeto arqueológico, paleontológico e geológico no médio curso do Ribeira de Iguape, SP." *Espeleo-Tema* 14: 22–35.
- Bequaert, J. 1948. "Monograph of the Strophocheilidae, a Neotropical Family of Terrestrial Mollusks." *Bulletin of the Museum of Comparative Zoology at Harvard College* 100, no. 1: 1–210.
- Beresford-Jones, D., D. Friesem, F. Sturt, et al. 2022. "Insights Into Changing Coastlines, Environments and Marine Hunter-Gatherer Lifestyles on the Pacific Coast of South America From the La Yerba II Shell Midden, Río Ica Estuary, Peru." *Quaternary Science Reviews* 285: 107509. <https://doi.org/10.1016/j.quascirev.2022.107509>.
- Berna, F., A. Behar, R. Shahack-Gross, et al. 2007. "Sediments Exposed to High Temperatures: Reconstructing Pyrotechnological Processes in Late Bronze and Iron Age Strata at Tel Dor (Israel)." *Journal of Archaeological Science* 34, no. 3: 358–373. <https://doi.org/10.1016/j.jas.2006.05.011>.
- Berna, F., A. Matthews, and S. Weiner. 2004. "Solubilities of Bone Mineral From Archaeological Sites: The Recrystallization Window." *Journal of Archaeological Science* 31, no. 7: 867–882. <https://doi.org/10.1016/j.jas.2003.12.003>.
- Bernal, J. P., F. W. Cruz, N. M. Strikis, et al. 2016. "High-Resolution Holocene South American Monsoon History Recorded by a Speleothem From Botuverá Cave, Brazil." *Earth and Planetary Science Letters* 450: 186–196. <https://doi.org/10.1016/j.epsl.2016.06.008>.
- Bernáldez-Sánchez, E., and E. García-Iñás. 2014. "Deposits of Terrestrial Snails: Natural or Anthropogenic Processes?" In *Archaeomalacology: Shells in the Archaeological Record*, edited by K. Szabó, C. Dupont, V. Dimitrijević, L. Gastéllum, and N. Serrand, 235–244. Archaeopress.
- Bishop, R. L. 2017. "Neutron Activation Analysis." In *Encyclopedia of Geoarchaeology*, edited by A. S. Gilbert, P. Goldberg, V. T. Holliday, R. D. Mandel, and R. S. Sternberg, 543–546. Springer Science+Business Media. https://doi.org/10.1007/978-1-4020-4409-0_20.
- Bode, P. 2017. "Neutron Activation Analysis (NAA)." In *Neutron Methods for Archaeology and Cultural Heritage*, edited by N. Kardjilov and G. Festa, 209–219. Springer Nature. https://doi.org/10.1007/978-3-319-33163-8_10.
- Bonizzoni, L., S. Bruni, A. Girod, and V. Guglielmi. 2009. "Archaeometric Study of Shells of Helicidae From the Edera Cave (Northeastern Italy)." *Archaeometry* 51, no. 1: 151–173. <https://doi.org/10.1111/j.1475-4754.2008.00412.x>.
- Braadbaart, F., and I. Poole. 2008. "Morphological, Chemical and Physical Changes During Charcoalification of Wood and Its Relevance to Archaeological Contexts." *Journal of Archaeological Science* 35, no. 9: 2434–2445. <https://doi.org/10.1016/j.jas.2008.03.016>.
- Braadbaart, F., I. Poole, H. Huisman, and B. van Os. 2012. "Fuel, Fire and Heat: An Experimental Approach to Highlight the Potential of Studying Ash and Char Remains From Archaeological Contexts." *Journal of Archaeological Science* 39: 836–847. <https://doi.org/10.1016/j.jas.2011.10.009>.
- Bullock, P., N. Fedoroff, A. Jongerius, G. Stoops, T. Tursina, and U. Babel. 1985. *Handbook for Soil Thin Section Description*. Wayne Research.
- Burns, A., M. D. Pickering, K. A. Green, et al. 2017. "Micromorphological and Chemical Investigation of Late-Viking Age Grave Fills at Hofstaðir, Iceland." *Geoderma* 306: 183–194. <https://doi.org/10.1016/j.geoderma.2017.06.021>.
- Calippo, F. 2004. "Os sambaquis submersos de Cananéia: um estudo de caso de arqueologia subaquática." Master's diss., University of São Paulo. <https://teses.usp.br/teses/disponiveis/8/8153/tde-27062006-143634/ptbr.php>.
- Camargo, O. A., A. C. Moniz, J. A. Jorge, and J. Valadares. 2009. *Métodos de análise química, mineralógica e física de solos do Instituto Agrônomo de Campinas. Boletim Técnico do Instituto Agrônomo de Campinas*. Instituto Agrônomo de Campinas.
- Campanha, G., and G. Sadowski. 1999. "Tectonics of the Southern Portion of the Ribeira Belt (Apiá Domain)." *Precambrian Research* 98, no. 1–2: 31–51. [https://doi.org/10.1016/S0301-9268\(99\)00027-3](https://doi.org/10.1016/S0301-9268(99)00027-3).
- Campanili, M., and W. Schaffer. 2010. *Mata Atlântica: patrimônio nacional dos brasileiros*. Ministério do Meio Ambiente.
- Canti, M., and J. Brochier. 2017. "Plant Ash." In *Archaeological Soil and Sediment Micromorphology*, edited by C. Nicosia and G. Stoops, 147–154. Wiley Blackwell. <https://doi.org/10.1002/9781118941065.ch17>.
- Canti, M. G. 2003. "Aspects of the Chemical and Microscopic Characteristics of Plant Ashes Found in Archaeological Soils." *Catena* 54, no. 3: 339–361. [https://doi.org/10.1016/S0341-8162\(03\)00127-9](https://doi.org/10.1016/S0341-8162(03)00127-9).
- Chahud, A., P. R. Oliveira Costa, G. F. Figueiredo, and M. M. M. Okumura. 2023. "Quaternary Ungulates of the Abismo Ponta de Flecha Cave, Ribeira of Iguape Valley, Southeast Brazil: Zooarchaeological and Paleoenvironmental Aspects." *Journal of South American Earth Sciences* 121: 104107. <https://doi.org/10.1016/j.jsames.2022.104107>.
- Cheng, H., H. Zhang, C. Spötl, et al. 2020. "Timing and Structure of the Younger Dryas Event and Its Underlying Climate Dynamics." *Proceedings of the National Academy of Sciences United States of America* 117: 23408–23417. <https://doi.org/10.1073/pnas.2007869117>.
- Chukanov, N. 2014. *Infrared Spectra of Mineral Species: Extended Library*. Springer Netherlands.
- Claassen, C. 2010. *Feasting With Shellfish in the Southern Ohio Valley: Archaic Sacred Sites and Rituals*. The University of Tennessee Press.
- Collet, G.-C. 1978a. *Notas prévias sobre sondagens efetuadas num abrigo sobre rocha no vale do rio Maximiano-Iporanga-SP*. Sociedade Brasileira de Espeleologia.

- Collet, G.-C. 1978b. *Notas prévias sobre sondagens efetuadas num abrigo sobre rocha no vale do rio Maximiano-Iporanga-SP. Segunda fase e conclusões*. Sociedade Brasileira de Espeleologia.
- Collet, G.-C. 1985. "Novas informações sobre os sambaquis fluviais do Estado de São Paulo." *Arquivos do Museu de História Natural da UFMG* 10: 311–324.
- Collet, G.-C. 2001. "O primeiro povoamento da América do Sul." In *13th International Congress of Speleology—4th Speleological Congress of Latin America and Caribbean—26th Brazilian Congress of Speleology*, 339–343. Union Internationale de Spéléologie—Federación Espeleológica de América Latina y del Caribe—SBE.
- Collet, G.-C., and C. M. Guimarães. 1977. "Resultado da sondagem do sambaqui Januário." *Arquivos do Museu de História Natural da UFMG* 2: 36–50.
- Collet, G.-C., and A. Prous. 1977. "Primeiro informe sobre os sambaquis fluviais da região de Itaoca (SP)." *Arquivos do Museu de História Natural da UFMG* 2: 31–35.
- Collinson, J. D., N. P. Mountney, and D. B. Thompson. 2006. *Sedimentary Structures*. Terra Publishing.
- Courty, M.-A., P. Goldberg, and R. Macphail. 1989. *Soils and Micro-morphology in Archaeology*. Cambridge University Press.
- Crema, E. R., and A. Bevan. 2021. "Inference From Large Sets of Radiocarbon Dates: Software and Methods." *Radiocarbon* 63: 23–39. <https://doi.org/10.1017/RDC.2020.95>.
- Cruz, F. W., S. J. Burns, I. Karmann, W. D. Sharp, and M. Vuille. 2006. "Reconstruction of Regional Atmospheric Circulation Features During the Late Pleistocene in Subtropical Brazil From Oxygen Isotope Composition of Speleothems." *Earth and Planetary Science Letters* 248: 495–507. <https://doi.org/10.1016/j.epsl.2006.06.019>.
- DeBlasis, P. A. D. 1988. "A ocupação pré-colonial do vale do Ribeira de Iguape, SP: os sítios líticos do médio curso." Unpublished Master's diss., University of São Paulo.
- DeBlasis, P. A. D. 1996. "Bairro da Serra em três tempos: arqueologia, uso do espaço regional e continuidade cultural no médio vale do Ribeira." Unpublished Doctoral thesis., University of São Paulo.
- DeBlasis, P. A. D. 1999. "Indicadores da transição do Arcaico para o Formativo na região montanhosa do médio vale do Ribeira, SP." In *Pré-história da Terra Brasilis*, edited by M. Tenório, 273–284. Editora da Universidade Federal de Rio de Janeiro.
- DeBlasis, P., M. Gaspar, and A. Kneip. 2021. "Sambaquis From the Southern Brazilian Coast: Landscape Building and Enduring Heterarchical Societies Throughout the Holocene." *Land* 10: 757. <https://doi.org/10.3390/land10070757>.
- DeBlasis, P. A. D., S. Piedade, and W. Morales. 1994. "Algumas considerações sobre os sambaquis fluviais do Médio Ribeira, SP." *Revista do Museu de Arqueologia e Etnologia* 4: 218. <https://doi.org/10.11606/issn.2448-1750.revmae.1994.109208>.
- Deininger, M., B. M. Ward, V. F. Novello, and F. W. Cruz. 2019. "Late Quaternary Variations in the South American Monsoon System as Inferred by Speleothems: New Perspectives Using the SISAL Database." *Quaternary* 2: 1–21. <https://doi.org/10.3390/quat2010006>.
- Duarte, C., E. Iriarte, M. Diniz, and P. Arias. 2019. "The Microstratigraphic Record of Human Activities and Formation Processes at the Mesolithic Shell Midden of Poças de São Bento (Sado Valley, Portugal)." *Archaeological and Anthropological Sciences* 11, no. 2: 483–509. <https://doi.org/10.1007/s12520-017-0519-0>.
- Etiégni, L., and A. Campbell. 1991. "Physical and Chemical Characteristics of Wood Ash." *Bioresource Technology* 37: 173–178. [https://doi.org/10.1016/0960-8524\(91\)90207-Z](https://doi.org/10.1016/0960-8524(91)90207-Z).
- Faleiros, F., Morais, S., and Costa, V., eds. 2012. *Geologia e recursos minerais da Folha Apiaí - SG.22-X-B-V, escala 1:100.000, estados de São Paulo e Paraná*. CPRM - Serviço Geológico do Brasil.
- Felizardo, A. 2017. "Abrigo Maximiano: uma análise sob a ótica da geoarqueologia." Master's diss., University of São Paulo. <https://teses.usp.br/teses/disponiveis/71/71131/tde-30012018-122308/pt-br.php>.
- Ferraz, T., X. Villagran, K. Nägele, et al. 2023. "Genomic History of Coastal Societies From Eastern South America." *Nature Ecology & Evolution* 7: 1315–1330. <https://doi.org/10.1038/s41559-023-02114-9>.
- Figuti, L., and C. Plens. 2014. "The Riverine Sambaqui: Zooarchaeological Studies of Inland Brazilian Shell-Mounds." In *The Cultural Dynamics of Shell-Matrix Sites*, edited by M. Roksandic, S. Mendonça de Souza, S. Eggers, M. Burchell, and D. Klokler, 213–222. University of New Mexico Press.
- Figuti, L., C. Plens, and P. DeBlasis. 2013. "Small Sambaquis and Big Chronologies: Shellmound Building and Hunter-Gatherers in Neotropical Highlands." *Radiocarbon* 55: 1215–1221. <https://doi.org/10.1017/S0033822200048128>.
- Flügel, E. 2004. *Microfacies of Carbonate Rocks. Analysis, Interpretation and Application*. Springer-Verlag.
- Fontenelle, J., and M. Miranda. 2017. "Aspects of Biology of Megalobolimus Paranaguensis (Gastropoda, Acavoidea) in the Coastal Plain of the Brazilian Southeast." *Iheringia. Série Zoologia* 107: 1–5. <https://doi.org/10.1590/1678-4766e2017004>.
- Forget, M., L. Regev, D. Friesem, and R. Shahack-Gross. 2015. "Physical and Mineralogical Properties of Experimentally Heated Chaff-Tempered Mud Bricks: Implications for Reconstruction of Environmental Factors Influencing the Appearance of Mud Bricks in Archaeological Conflagration Events." *Journal of Archaeological Science: Reports* 2: 80–93. <https://doi.org/10.1016/j.jasrep.2015.01.008>.
- Frascá, M. 1993. "Petrografia e geoquímica de rochas carbonáticas pré-cambrianas do Estado de São Paulo." Master's diss., University of São Paulo. <https://www.teses.usp.br/teses/disponiveis/44/44135/tde-20082013-090303/pt-br.php>.
- French, C. 2022. *Human Transformations of the Earth*. Oxbow Books.
- French, C., and T. Rajkovača. 2015. "A Brief Guide to Making Soil/Sediment Thin Sections: From the Field to Finished Slide Using the Brot Grinding System." In *A Handbook of Geoarchaeological Approaches for Investigating Landscapes and Settlement Sites*, edited by C. French, 97–100. Oxbow Books.
- Friesem, D., N. Lavi, M. Madella, P. Ajithprasad, and C. French. 2016. "Site Formation Processes and Hunter-Gatherers Use of Space in a Tropical Environment: A Geo-Ethnoarchaeological Approach From South India." *PLoS One* 11, no. 10: e0164185. <https://doi.org/10.1371/journal.pone.0164185>.
- Friesem, D., N. Lavi, M. Madella, E. Boaretto, P. Ajithprasad, and C. French. 2017. "The Formation of Fire Residues Associated With Hunter-Gatherers in Humid Tropical Environments: A Geo-Ethnoarchaeological Perspective." *Quaternary Science Reviews* 171: 85–99. <https://doi.org/10.1016/j.quascirev.2017.07.002>.
- Friesem, D., R. Shahack-Gross, M. Weinstein-Evron, N. Teutsch, L. Weissbrod, and R. Shimelmitz. 2021. "High-Resolution Study of Middle Palaeolithic Deposits and Formation Processes at Tabun Cave, Israel: Guano-Rich Cave Deposits and Detailed Stratigraphic Appreciation of Layer C." *Quaternary Science Reviews* 274: 107203. <https://doi.org/10.1016/j.quascirev.2021.107203>.
- Fundação Florestal. 2010. *Parque Estadual Turístico do Alto Ribeira—PETAR*. Plano de Manejo Espeleológico.
- Fundação Florestal. 2018. *Parque Estadual Turístico do Alto Ribeira—PETAR*. Plano de Manejo.
- Fundação SOS Mata Atlântica. 2023. *Atlas dos remanescentes florestais da Mata Atlântica: período 2021-2022*. Fundação SOS Mata Atlântica-Instituto Nacional de Pesquisas Espaciais.

- Furquim, L., J. Watling, L. Hilbert, et al. 2021. "Facing Change Through Diversity: Resilience and Diversification of Plant Management Strategies During the Mid to Late Holocene Transition at the Monte Castelo Shellmound, SW Amazonia." *Quaternary* 4: 1–8. <https://doi.org/10.3390/quat4010008>.
- Gallelo, G., A. Pastor, A. Diez, N. La Roca, and J. Bernabeu. 2013. "Anthropogenic Units Fingerprinted by REE in Archaeological Stratigraphy: Mas d'is (Spain) Case." *Journal of Archaeological Science* 40, no. 2: 799–809. <https://doi.org/10.1016/j.jas.2012.10.005>.
- García, P., Y. Zaidner, C. Nicosia, and R. Shahack-Gross. 2024. "Site Formation Processes at Tinsmet Cave, Israel: Micro-Stratigraphy, Fire Use, and Cementation." *Geoarchaeology* 40: e22023. <https://doi.org/10.1002/gea.22023>.
- Gaspar, M., P. DeBlasis, S. Fish, and P. Fish. 2008. "Sambaqui (Shell Mound) Societies of Coastal Brazil." In *Handbook of South American Archaeology*, edited by H. Silverman and W. Isbell, 319–335. Springer.
- Gaspar, M., D. Klokler, and P. DeBlasis. 2014. "Were Sambaqui People Buried in the Trash? Archaeology, Physical Anthropology, and the Evolution of the Interpretation of Brazilian Shell Mounds." In *The Cultural Dynamics of Shell-Matrix Sites*, edited by M. Roksandic, S. Mendonça de Souza, S. Eggers, M. Burchell, and D. Klokler, 91–100. University of New Mexico Press.
- Gé, T., M.-A. Courty, W. Matthews, and J. Wattez. 1993. "Sedimentary Formation Processes of Occupation Surfaces." In *Formation Processes in Archaeological Context*, edited by P. Goldberg, D. Nash, and M. Petraglia, 149–163. Prehistory Press.
- Girod, A. 2011. "Land Snails From Late Glacial and Early Holocene Italian Sites." *Quaternary International* 244: 105–116. <https://doi.org/10.1016/j.quaint.2011.04.025>.
- Glascok, M. 2019. "Compositional Analysis of Archaeological Ceramics." In *Ceramics of the Indigenous Cultures of South America: Studies of Production and Exchange Through Compositional Analysis*, edited by M. Glascok, H. Neff, and K. Vaughn, 1–13. University of New Mexico Press.
- Glascok, M., and H. Neff. 2003. "Neutron Activation Analysis and Provenance Research in Archaeology." *Measurement Science and Technology* 14, no. 9: 1516–1526. <https://doi.org/10.1088/0957-0233/14/9/304>.
- Goldberg, P. 2000. "Micromorphology and Site Formation at Die Kelders Cave I, South Africa." *Journal of Human Evolution* 38: 43–90. <https://doi.org/10.1006/jhev.1999.0350>.
- Goldberg, P., and V. Aldeias. 2018. "Why Does (Archaeological) Micromorphology Have Such Little Traction in (Geo)Archaeology?" *Archaeological and Anthropological Sciences* 10: 269–278. <https://doi.org/10.1007/s12520-016-0353-9>.
- Goldberg, P., and R. Macphail. 2003. "Short Contribution: Strategies and Techniques in Collecting Micromorphology Samples." *Geoarchaeology* 18: 571–578. <https://doi.org/10.1002/gea.10079>.
- Goldberg, P., and R. I. Macphail. 2006. *Practical and Theoretical in Geoarchaeology*. Blackwell Publishing.
- Goldberg, P., C. Miller, S. Schiegl, et al. 2009. "Bedding, Hearths, and Site Maintenance in the Middle Stone Age of Sibudu Cave, KwaZulu-Natal, South Africa." *Archaeological and Anthropological Sciences* 1: 95–122. <https://doi.org/10.1007/s12520-009-0008-1>.
- Grono, E., D. Friesem, T. Lam, et al. 2022. "Microstratigraphy Reveals Cycles of Occupation and Abandonment at the Mid Holocene Coastal Site of Thach Lac, Northern-Central Vietnam." *Archaeological Research in Asia* 31: 100396. <https://doi.org/10.1016/j.ara.2022.100396>.
- Haaland, M., C. Miller, O. Unhammer, et al. 2021. "Geoarchaeological Investigation of Occupation Deposits in Blombos Cave in South Africa Indicate Changes in Site Use and Settlement Dynamics in the Southern Cape During MIS 5b-4." *Quaternary Research* 100: 170–223. <https://doi.org/10.1017/qua.2020.75>.
- Hale, J. C., J. Benjamin, K. Woo, et al. 2021. "Submerged Landscapes, Marine Transgression and Underwater Shell Middens: Comparative Analysis of Site Formation and Taphonomy in Europe and North America." *Quaternary Science Reviews* 258: 106867. <https://doi.org/10.1016/j.quascirev.2021.106867>.
- Heiri, O., A. Lotter, and G. Lemcke. 2001. "Loss on Ignition as a Method for Estimating Organic and Carbonate Content in Sediments: Reproducibility and Comparability of Results." *Journal of Paleolimnology* 25: 101–110. <https://doi.org/10.1023/A:1008119611481>.
- Hogg, A., T. Heaton, Q. Hua, et al. 2020. "SHCal20 Southern Hemisphere Calibration, 0–55,000 Years Cal BP." *Radiocarbon* 62, no. 4: 759–778. <https://doi.org/10.1017/RDC.2020.59>.
- Homsey, L., and R. Capo. 2006. "Integrating Geochemistry and Micromorphology to Interpret Feature Use at Dust Cave, a Paleo-Indian Through Middle-Archaic Site in Northwest Alabama." *Geoarchaeology* 21, no. 3: 237–269. <https://doi.org/10.1002/gea.20103>.
- Hunt, C., and E. Hill. 2017. "Caves and Molluscs." In *Molluscs in Archaeology: Methods, Approaches and Applications*, edited by M. Allen, 100–110. Oxbow Books. <https://doi.org/10.2307/j.ctvh1dk5s.12>.
- Ismail-Meyer, K., M. H. Stolt, and D. L. Lindbo. 2018. "Soil Organic Matter." In *Interpretation of Micromorphological Features of Soils and Regoliths*, edited by G. Stoops, V. Marcelino, and F. Mees, 471–512. Elsevier. <https://doi.org/10.1016/B978-0-444-63522-8.00017-6>.
- Ivanauskas, N., R. Miashike, J. Godoy, et al. 2012. "A vegetação do Parque Estadual Turístico do Alto Ribeira (PETAR), São Paulo, Brasil." *Biota Neotropica* 12, no. 1: 147–177. <https://doi.org/10.1590/S1676-06032012000100013>.
- Karkanas, P. 2010. "Preservation of Anthropogenic Materials Under Different Geochemical Processes: A Mineralogical Approach." *Quaternary International* 214: 63–69. <https://doi.org/10.1016/j.quaint.2009.10.017>.
- Karkanas, P. 2021. "All About Wood Ash: Long Term Fire Experiments Reveal Unknown Aspects of the Formation and Preservation of Ash With Critical Implications on the Emergence and Use of Fire in the Past." *Journal of Archaeological Science* 135: 105476. <https://doi.org/10.1016/j.jas.2021.105476>.
- Karkanas, P., O. Bar-Yosef, P. Goldberg, and S. Weiner. 2000. "Diagenesis in Prehistoric Caves: The Use of Minerals That Form In Situ to Assess the Completeness of the Archaeological Record." *Journal of Archaeological Science* 27: 915–929. <https://doi.org/10.1006/jasc.1999.0506>.
- Karkanas, P., K. Brown, E. Fisher, Z. Jacobs, and C. Marean. 2015. "Interpreting Human Behavior From Depositional Rates and Combustion Features Through the Study of Sedimentary Microfacies at Site Pinnacle Point 5-6, South Africa." *Journal of Human Evolution* 85: 1–21. <https://doi.org/10.1016/j.jhevol.2015.04.006>.
- Karkanas, P., and P. Goldberg. 2018. *Reconstructing Archaeological Sites: Understanding the Geoarchaeological Matrix*. Wiley.
- Karkanas, P., J.-P. Rigaud, J. Simek, R. Albert, and S. Weiner. 2002. "Ash Bones and Guano: A Study of the Minerals and Phytoliths in the Sediments of Grotte XVI, Dordogne, France." *Journal of Archaeological Science* 29: 721–732. <https://doi.org/10.1006/jasc.2001.0742>.
- Karmann, I., and J. Ferrari. 2002. "Carste e cavernas do Parque Estadual Turístico do Alto Ribeira (PETAR), SP: sistemas de cavernas com paisagens subterrâneas únicas." In *Sítios geológicos e paleontológicos do Brasil*, edited by C. Schobbenhaus, D. Campos, E. Queiroz, M. Winge, and M. Berbert-Born, 401–413. Departamento Nacional de Produção Mineral—Serviço Geológico do Brasil.
- Klokler, D. 2014. "A Ritually Constructed Shell Mound: Feasting at the Jabuticabeira II site." In *The Cultural Dynamics of Shell-Matrix Sites*, edited by M. Roksandic, S. Mendonça de Souza, S. Eggers, M. Burchell, and D. Klokler, 151–162. University of New Mexico Press.
- Kooistra, M., and M. Pulleman. 2018. "Features Related to Faunal Activity." In *Interpretation of Micromorphological Features of Soils and*

- Regoliths*, edited by G. Stoops, V. Marcelino, and F. Mees, 447–469. Elsevier. <https://doi.org/10.1016/B978-0-444-63522-8.00016-4>.
- Kourampas, N., I. A. Simpson, N. Perera, S. U. Deraniyagala, and W. H. Wijeyapala. 2009. "Rockshelter Sedimentation in a Dynamic Tropical Landscape: Late Pleistocene–Early Holocene Archaeological Deposits in Kitulgala Beli-Lena, Southwestern Sri Lanka." *Geoarchaeology* 24: 677–714. <https://doi.org/10.1002/gea.20287>.
- Kovda, I., and A. R. Mermut. 2018. "Vertic Features." In *Interpretation of Micromorphological Features of Soils and Regoliths*, edited by G. Stoops, V. Marcelino, and F. Mees, 605–632. Elsevier. <https://doi.org/10.1016/B978-0-444-63522-8.00021-8>.
- Krone, R. 1909. *As grutas calcareas do valle do rio Ribeira de Iguape (Illustrada com 42 gravuras e um mappa topographico)*. Imprensa Nacional.
- Ledru, M.-P., V. Montade, G. Blanchard, and C. Hély. 2015. "Long-Term Spatial Changes in the Distribution of the Brazilian Atlantic Forest." *Biotropica* 48: 159–169. <https://doi.org/10.1111/btp.12266>.
- Lenhare, B. D., and W. Sallun Filho. 2014. "O carste nas cabeceiras dos rios das Almas, São José de Guapiara (Planalto de Guapiara) e do rio Pilões (Serra de Paranapiacaba), SP." *Geociências* 33: 686–700.
- Linstädter, J., and M. Kehl. 2012. "The Holocene Archaeological Sequence and Sedimentological Processes at Ifri Oudadane, NE Morocco." *Journal of Archaeological Science* 39: 3306–3323. <https://doi.org/10.1016/j.jas.2012.05.025>.
- Lloveras, L., J. Nadal, P. Argüelles, J. Fullola, and A. Estrada. 2011. "The Land Snail Midden From Balma del Gai (Barcelona, Spain) and the Evolution of Terrestrial Gastropod Consumption During the Late Palaeolithic and Mesolithic in Eastern Iberia." *Quaternary International* 244, no. 1: 37–44. <https://doi.org/10.1016/j.quaint.2011.04.036>.
- Lombardo, U., K. Szabó, J. M. Capriles, et al. 2013. "Early and Middle Holocene Hunter-Gatherer Occupations in Western Amazonia: The Hidden Shell Middens." *PLoS One* 8: e72746. <https://doi.org/10.1371/journal.pone.0072746>.
- Lubell, D. 2004. "Prehistoric Edible Land Snails in the Circum-Mediterranean: The Archaeological Evidence." In *Petits animaux et sociétés humaines. Du complément alimentaire aux ressources utilitaires. XXIVe rencontres internationales d'archéologie et d'histoire d'Antibes*, edited by J.-P. Brugal and J. Desse, 77–98. Éditions APDCA.
- Lubell, D., F. A. Hassan, A. Gautier, and J.-L. Ballais. 1976. "The Capsian Escargotières: An Interdisciplinary Study Elucidates Holocene Ecology and Subsistence in North Africa." *Science* 191: 910–920. <https://doi.org/10.1126/science.191.4230.910>.
- Macphail, R. I., M. A. Courty, J. Hather, and J. Wattez. 1997. "The Soil Micromorphological Evidence of Domestic Occupation and Stabling Activities." In *Arene Candide: A Functional and Environmental Assessment of the Holocene Sequence. Excavations Bernabò Brea-Cardini 1940–50*, edited by R. Maggi, E. Starnini, and B. Voytek, 53–88. Il Calamo.
- Madejová, J. 2003. "FTIR Techniques in Clay Mineral Studies." *Vibrational Spectroscopy* 31, no. 1: 1–10. [https://doi.org/10.1016/S0924-2031\(02\)00065-6](https://doi.org/10.1016/S0924-2031(02)00065-6).
- Mallol, C., and P. Goldberg. 2017. "Cave and Rockshelter Sediments." In *Archaeological Soil and Sediment Micromorphology*, edited by C. Nicosia and G. Stoops, 359–381. Wiley Blackwell. <https://doi.org/10.1002/9781118941065.ch34>.
- Mallol, C., C. Hernández, D. Cabanes, et al. 2013. "Human Actions Performed on Simple Combustion Structures: An Experimental Approach to the Study of Middle Palaeolithic Fire." *Quaternary International* 315: 3–15. <https://doi.org/10.1016/j.quaint.2013.04.009>.
- Mallol, C., S. Mentzer, and C. Miller. 2017. "Combustion Features." In *Archaeological Soil and Sediment Micromorphology*, edited by C. Nicosia and G. Stoops, 299–330. Wiley Blackwell. <https://doi.org/10.1002/9781118941065.ch31>.
- Marcazzan, D., C. Miller, and N. Conard. 2022. "Burning, Dumping, and Site Use During the Middle and Upper Palaeolithic at Hohle Fels Cave, SW Germany." *Archaeological and Anthropological Sciences* 14, no. 9: 178. <https://doi.org/10.1007/s12520-022-01647-7>.
- Matthews, W., C. French, T. Lawrence, D. Cutler, and M. Jones. 1997. "Microstratigraphic Traces of Site Formation Processes and Human Activities." *World Archaeology* 29: 281–308. <https://doi.org/10.1080/00438243.1997.9980378>.
- McAdams, C., M. Morley, X. Fu, et al. 2020. "The Pleistocene Geoarchaeology and Geochronology of Con Moong Cave, North Vietnam: Site Formation Processes and Hominin Activity in the Humid Tropics." *Geoarchaeology* 35: 72–97. <https://doi.org/10.1002/gea.21758>.
- McAdams, C., M. W. Morley, X. Fu, et al. 2022. "Late Pleistocene Shell Midden Microstratigraphy Indicates a Complex History of Human–Environment Interactions in the Uplands of Northern Vietnam." *Philosophical Transactions of the Royal Society B* 377: 20200493. <https://doi.org/10.1098/rstb.2020.0493>.
- Meinekat, S., C. Miller, and K. Rademaker. 2022. "A Site Formation Model for Cuncacha Rock Shelter: Depositional and Postdepositional Processes at the High-Altitude Keysite in the Peruvian Andes." *Geoarchaeology* 37, no. 2: 304–331. <https://doi.org/10.1002/gea.21889>.
- Mentzer, S. 2014. "Microarchaeological Approaches to the Identification and Interpretation of Combustion Features in Prehistoric Archaeological Sites." *Journal of Archaeological Method and Theory* 21, no. 3: 616–668. <https://doi.org/10.1007/s10816-012-9163-2>.
- Middleton, W. D., and D. T. Price. 1996. "Identification of Activity Areas by Multi-Element Characterization of Sediments From Modern and Archaeological House Floors Using Inductively Coupled Plasma-Atomic Emission Spectroscopy." *Journal of Archaeological Science* 23: 673–687. <https://doi.org/10.1006/jasc.1996.0064>.
- Milek, K. 2012. "Floor Formation Processes and the Interpretation of Site Activity Areas: An Ethnoarchaeological Study of Turf Buildings at Thverá, Northeast Iceland." *Journal of Anthropological Archaeology* 31, no. 2: 119–137. <https://doi.org/10.1016/j.jaa.2011.11.001>.
- Milek, K., and C. French. 2007. "Soils and Sediments in the Settlement and Harbour at Kaupang." In *Kaupang in Skiringssal: Kaupang Excavation Project Publication Series*, edited by D. Skre, 321–360. Aarhus University Press.
- Milek, K., and H. Roberts. 2013. "Integrated Geoarchaeological Methods for the Determination of Site Activity Areas: A Study of a Viking Age House in Reykjavik, Iceland." *Journal of Archaeological Science* 40: 1845–1865. <https://doi.org/10.1016/j.jas.2012.10.031>.
- Miller, C., N. Conard, P. Goldberg, and F. Berna. 2010. "Dumping, Sweeping and Trampling: Experimental Micromorphological Analysis of Anthropogenically Modified Combustion Features." *Palethnologie* 2, no. 2: 25–37.
- Miller, C., P. Goldberg, and F. Berna. 2013. "Geoarchaeological Investigations at Diepkloof Rock Shelter, Western Cape, South Africa." *Journal of Archaeological Science* 40: 3432–3452. <https://doi.org/10.1016/j.jas.2013.02.014>.
- Monnier, G. 2018. "A Review of Infrared Spectroscopy in Microarchaeology: Methods, Applications, and Recent Trends." *Journal of Archaeological Science: Reports* 18: 806–823.
- Moore, C., and V. Thompson. 2012. "Animism and Green River Persistent Places: A Dwelling Perspective of the Shell Mound Archaic." *Journal of Social Archaeology* 12: 264–284. <https://doi.org/10.1177/1469605311431518>.
- Morley, M., and P. Goldberg. 2017. "Geoarchaeological Research in the Humid Tropics: A Global Perspective." *Journal of Archaeological Science* 77: 1–9. <https://doi.org/10.1016/j.jas.2016.11.002>.
- Morley, M. W. 2017. "The Geoarchaeology of Hominin Dispersals to and From Tropical Southeast Asia: A Review and Prognosis." *Journal of Archaeological Science* 77: 78–93. <https://doi.org/10.1016/j.jas.2016.07.009>.

- Morrissey, P., S. M. Mentzer, and S. Wurz. 2023. "The Stratigraphy and Formation of Middle Stone Age Deposits in Cave 1B, Klasies River Main Site, South Africa, With Implications for the Context, Age, and Cultural Association of the KRM 41815/SAM-AP 6222 Human Mandible." *Journal of Human Evolution* 183: 103414. <https://doi.org/10.1016/j.jhevol.2023.103414>.
- Moss, G., and M. Moss. 2007. *Projeto Brasil das Águas - Sete rios: Ribeira. Petrobrás*.
- Munita, C. S., N. Batalla, A. F. Costa, et al. 2020. "Explorando problemas arqueológicos com técnicas físico-químicas: A trajetória do Grupo de Estudos Arqueométricos do Instituto de Pesquisas Energéticas e Nucleares, São Paulo, Brasil." *Boletim do Museu Paraense Emílio Goeldi. Ciências Humanas* 15: e20200004. <https://doi.org/10.1590/2178-2547-BGOELDI-2020-0004>.
- Munita, C. S., M. D. Glascock, and R. Hazenfratz. 2019. "Neutron Activation Analysis: An Overview." In *Recent Advances in Analytical Techniques*, edited by A.-U. Rahman and S. A. Ozkan, 3, 179–227. Bentham Science Publishers. <https://doi.org/10.2174/9781681085722119030007>.
- Nascimento, D., M. Chiapini, P. Vidal-Torrado, et al. 2024. "The Underestimated Role of Leaf-Cutting Ants in Soil and Geomorphological Development in Neotropical America." *Earth-Science Reviews* 248: 104650. <https://doi.org/10.1016/j.earscirev.2023.104650>.
- Needham, S., and T. Spence. 1997. "Refuse and the Formation of Middens." *Antiquity* 71: 77–90. <https://doi.org/10.1017/S0003598X00084568>.
- Neves, W. A., M. Hubbe, M. M. M. Okumura, et al. 2005. "A New Early Holocene Human Skeleton From Brazil: Implications for the Settlement of the New World." *Journal of Human Evolution* 48: 403–414. <https://doi.org/10.1016/j.jhevol.2004.12.001>.
- Nicosia, C. and Stoops, G., eds. 2017. *Archaeological Soil and Sediment Micromorphology*. Wiley Blackwell.
- Ogloblin Ramirez, I., Z. C. Dunseth, D. Shalem, and R. Shahack-Gross. 2023. "Infrared Spectra of Mixtures of Heated and Unheated Clay: Solving an Interpretational Conundrum." *Geoarchaeology* 38: 822–829. <https://doi.org/10.1002/gea.21976>.
- de Oliveira, P. E., M. J. Garcia, V. B. Medeiros, et al. 2014. "Paleoclimas e paleovegetação do Quaternário no Estado de São Paulo, Brasil." In *Paleontologia: Cenários de vida*, edited by I. Souza Carvalho, M. J. Garcia, O. Strohschoen, Jr., C. C. Lana, 5, 457–470. Editora Interciência.
- Parellada, C. 2006. "Estudo arqueológico no alto vale do rio Ribeira: área do Gasoduto Bolívia-Brasil, trecho X, Paraná." Doctoral thesis, University of São Paulo. <https://teses.usp.br/teses/disponiveis/71/71131/tde-28072006-173819/pt-br.php>.
- Penin, A. 2005. "Análise dos processos formativos do Sítio Capelinha—estabelecimento de um contexto microrregional." Master's diss., University of São Paulo. <https://www.teses.usp.br/teses/disponiveis/71/71131/tde-19102006-153609/pt-br.php>.
- Pessenda, L. C., P. E. De Oliveira, M. Moffato, et al. 2009. "The Evolution of a Tropical Rainforest/Grassland Mosaic in Southeastern Brazil Since 28,000 14C yr BP Based on Carbon Isotopes and Pollen Records." *Quaternary Research* 71: 437–452. <https://doi.org/10.1016/j.yqres.2009.01.008>.
- Plens, C. 2009. "O papel dos amontoados de conchas no sambaqui fluvial." *Revista de Arqueologia* 22, no. 2: 77–93.
- Power, X., L. Sitzia, S. Yrarrázaval, et al. 2022. "Ritual Stone-Built Architecture and Shell Midden Foundation: A Semisubterranean Structure in Hyperarid Atacama Desert Coast, Northern Chile." *Geoarchaeology* 37: 198–226. <https://doi.org/10.1002/gea.21857>.
- Pugliese, F., C. Zimpel Neto, and E. Neves. 2019. "What do Amazonian Shellmounds Tell us About the Long-Term Indigenous History of South America?" In *Encyclopedia of Global Archaeology*, 1–25. Springer International Publishing. https://doi.org/10.1007/978-3-319-51726-1_3030-2.
- R Core Team. 2021. *R: A Language and Environment for Statistical Computing. Version 4.0.4*. The R Foundation for Statistical Computing. <https://www.R-project.org/>.
- Rabett, R., J. Appleby, A. Blyth, et al. 2011. "Inland Shell Midden Site-Formation: Investigation Into a Late Pleistocene to Early Holocene Midden From Trảng An, Northern Vietnam." *Quaternary International* 239, no. 1–2: 153–169. <https://doi.org/10.1016/j.quaint.2010.01.025>.
- Rentzel, P., C. Nicosia, A. Gebhardt, D. Brönnimann, C. Pümpin, and K. Ismail-Meyer. 2017. "Trampling, Poaching and the Effect of Traffic." In *Archaeological Soil and Sediment Micromorphology*, edited by C. Nicosia and G. Stoops, 281–297. Wiley Blackwell. <https://doi.org/10.1002/9781118941065.ch30>.
- Rick, T. 2023. "Shell Midden Archaeology: Current Trends and Future Directions." *Journal of Archaeological Research* 32: 1–58. <https://doi.org/10.1007/s10814-023-09189-9>.
- Robrahn, E. M. 1988. "A ocupação pré-colonial do vale do Ribeira de Iguape, SP: Os sítios cerâmicos do médio curso." Unpublished Master's diss., University of São Paulo.
- RStudio Team. 2020. *RStudio: Integrated Development for R. Version 1.4.1106*. <http://www.rstudio.com/>.
- Saia, S. E. M. G., L. C. R. Pessenda, S. E. M. Gouveia, R. Aravena, and J. A. Bendassolli. 2008. "Last Glacial Maximum (LGM) Vegetation Changes in the Atlantic Forest, Southeastern Brazil." *Quaternary International* 184: 195–201. <https://doi.org/10.1016/j.quaint.2007.06.029>.
- Sakai, K. 1981. *Notas arqueológicas do Estado de São Paulo, Brasil*. Instituto Paulista de Arqueologia.
- Sallun, A. E. M., W. Sallun Filho, K. Suguio, et al. 2012. "Geochemical Evidence of the 8.2 ka Event and Other Holocene Environmental Changes Recorded in Paleolagoon Sediments, Southeastern Brazil." *Quaternary Research* 77: 31–43. <https://doi.org/10.1016/j.yqres.2011.09.007>.
- Schiegl, S., P. Goldberg, O. Bar-Yosef, and S. Weiner. 1996. "Ash Deposits in Hayonim and Kebara Caves, Israel: Macroscopic, Microscopic and Mineralogical Observations, and Their Archaeological Implications." *Journal of Archaeological Science* 23, no. 5: 763–781. <https://doi.org/10.1006/jasc.1996.0071>.
- Schiffer, M. 1987. *Formation Processes of the Archaeological Record*. University of New Mexico Press.
- Shahack-Gross, R., A. Ayalon, P. Goldberg, et al. 2008. "Formation Processes of Cemented Features in Karstic Cave Sites Revealed Using Stable Oxygen and Carbon Isotopic Analyses: A Case Study at Middle Paleolithic Amud Cave, Israel." *Geoarchaeology* 23: 43–62. <https://doi.org/10.1002/gea.20203>.
- Shahack-Gross, R., F. Berna, P. Karkanas, C. Lemorini, A. Gopher, and R. Barkai. 2014. "Evidence for the Repeated Use of a Central Hearth at Middle Pleistocene (300 ky Ago) Qesem Cave, Israel." *Journal of Archaeological Science* 44: 12–21. <https://doi.org/10.1016/j.jas.2013.11.015>.
- Shillito, L.-M., and P. Ryan. 2013. "Surfaces and Streets: Phytoliths, Micromorphology and Changing Use of Space at Neolithic Çatalhöyük (Turkey)." *Antiquity* 87: 684–700. <https://doi.org/10.1017/S0003598X00049395>.
- Shillito, L. -M., and W. Matthews. 2013. "Geoarchaeological Investigations of Midden-Formation Processes in the Early to Late Ceramic Neolithic Levels at Çatalhöyük, Turkey ca. 8550–8370 Cal BP." *Geoarchaeology* 28, no. 1: 25–49. <https://doi.org/10.1002/gea.21427>.
- Silva, F., M. Pearl Shock, G. Prestes Carneiro, et al. 2021. "Flautas, banhas e caxiris: os gestos e os materiais perecíveis do passado resgatados no presente." *Revista de Arqueologia* 34, no. 3: 255–282. <https://doi.org/10.24885/sab.v34i3.935>.
- Silva, F. B. R. 1985. "Os cambissolos da porção central da Província Estrutural da Mantiqueira e suas relações com os latossolos: Alteração e pedogênese." Unpublished Doctoral thesis., University of São Paulo.
- Silva, L. V. 2022. "Fogueiras da pré-história no vale do rio Taquaraçu: Análise geoarqueológica da matriz sedimentar da Lapa do Niáctor,

- Jaboticatubas, Minas Gerais." *Revista de Geografia/PPGEO/UFJF* 12: 108–122.
- Simões, C. D., and V. Aldeias. 2022. "Thermo-Microstratigraphy of Shells Reveals Invisible Fire Use and Possible Cooking in the Archaeological Record." *Frontiers in Earth Science* 10: 869487. <https://doi.org/10.3389/feart.2022.869487>.
- Simões, C. D., E. Iriarte, I. Gutiérrez-Zugasti, and P. Arias. 2024. "Carbonate Microfacies Reveal How Asturian Shell Middens Formed in the Mesolithic." *Quaternary Science Reviews* 342: 108898. <https://doi.org/10.1016/j.quascirev.2024.108898>.
- Sisa-López de Pablo, J., J. Watzek, R. Álvarez, A. Bach-Gómez, and M. Molist. 2022. "Combustion Features and Use of Space. A Micromorphological Approach to the Neolithic Occupation at Cova de les Pixarelles (Barcelona, Spain)." *Journal of Archaeological Science: Reports* 46: 103712. <https://doi.org/10.1016/j.jasrep.2022.103712>.
- Stein, J. 1992a. "Interpreting Stratification of a Shell Midden." In *Deciphering a Shell Midden*, edited by J. Stein, 71–93. Academic Press.
- Stein, J. 1992b. "The Analysis of Shell Middens." In *Deciphering a Shell Midden*, edited by J. Stein, 1–24. Academic Press.
- Stein, J., D. Green, and S. Sherwood. 2011. "Sediment Analysis." In *Is it a House? Archaeological Excavations at English Camp, San Juan Island, Washington*, edited by A. Taylor and J. Stein, 45–63. Burke Museum of Natural History and Culture.
- Stephens, M., J. Rose, and D. D. Gilbertson. 2017. "Post-Depositional Alteration of Humid Tropical Cave Sediments: Micromorphological Research in the Great Cave of Niah, Sarawak, Borneo." *Journal of Archaeological Science* 77: 109–124. <https://doi.org/10.1016/j.jas.2016.01.015>.
- Stoops, G. 2021. *Guidelines for Analysis and Description of Soil and Regolith Thin Sections*. Wiley-Soil Science Society of America. <https://doi.org/10.1002/9780891189763>.
- Stoops, G., Marcelino, V., and Mees, F., eds. 2018. *Interpretation of Micromorphological Features of Soils and Regoliths*. Elsevier. <https://doi.org/10.1016/C2014-0-01728-5>.
- Sulas, F., S. M. Kristiansen, and S. Wynne-Jones. 2019. "Soil Geochemistry, Phytoliths and Artefacts From an Early Swahili Daub House, Unguja Ukuu, Zanzibar." *Journal of Archaeological Science* 103: 32–45. <https://doi.org/10.1016/j.jas.2019.01.010>.
- Swan, D., J. Clague, and J. Luternauer. 1979. "Grain-Size Statistics II: Evaluation of Grouped Moment Measures." *Journal of Sedimentary Research* 49: 487–500. <https://doi.org/10.1306/212F7775-2B24-11D7-8648000102C1865D>.
- Szabó, K. 2017. "Shell Middens." In *Encyclopedia of Geoarchaeology*, edited by A. S. Gilbert, P. Goldberg, V. T. Holliday, R. D. Mandel, and R. S. Sternberg, 772–788. Springer Science+Business Media. https://doi.org/10.1007/978-1-4020-4409-0_146.
- Taylor, V., R. Barton, M. Bell, et al. 2011. "The Epipalaeolithic (Iberomaurusian) at Grotte des Pigeons (Taforalt), Morocco: A Preliminary Study of the Land Mollusca." *Quaternary International* 244, no. 1: 5–14. <https://doi.org/10.1016/j.quaint.2011.04.041>.
- Taylor, V., and M. Bell. 2017. "Land Mollusc Middens." In *Molluscs in Archaeology: Methods, Approaches and Applications*, edited by M. Allen, 195–212. Oxbow Books. <https://doi.org/10.2307/j.ctvh1dk5s.18>.
- Teixeira, P. C., Donagemma, G. K., Fontana, A., and Teixeira, W. G., eds. 2017. *Manual de métodos de análise de solo*. Embrapa.
- Teixeira, W., C. Plens, R. Macedo, and L. Figuti. 2012. "Caracterização de um perfil de solo desenvolvido no sambaqui fluvial Moraes, município de Miracatu—SP." *Revista do Museu de Arqueologia e Etnologia* 22: 181–194. <https://doi.org/10.11606/issn.2448-1750.revmae.2012.107417>.
- Thompson, V., W. Marquardt, A. Cherkinsky, et al. 2016. "From Shell Midden to Midden-Mound: The Geoarchaeology of Mound Key, an Anthropogenic Island in Southwest Florida, USA." *PLoS One* 11, no. 4: e0154611. <https://doi.org/10.1371/journal.pone.0154611>.
- Tognoli, A. 2016. "Zooarqueologia dos sambaquis fluviais—Caraça, Estreito, Tatupeva e Lageado IV: uma leitura da paisagem sambaquieira da região de Itaoca—Vale do Ribeira de Iguape." Master's diss., University of São Paulo. <https://teses.usp.br/teses/disponiveis/71/71131/tde-14072016-161333/pt-br.php>.
- Tudela, D., A. Araujo, S. Tatum, J. Mittani, and C. Munita. 2020. "Preliminary Evidence of Prehistoric Human Activity by Chemical Analysis of Sediments From Lapa Grande de Taquaraçu Archaeological Site Using INAA." *Journal of Radioanalytical and Nuclear Chemistry* 325: 725–736. <https://doi.org/10.1007/s10967-020-07217-2>.
- Vepraskas, M. J., D. L. Lindbo, and M. H. Stolt. 2018. "Redoximorphic Features." In *Interpretation of Micromorphological Features of Soils and Regoliths*, edited by G. Stoops, V. Marcelino, and F. Mees, 425–445. Elsevier. <https://doi.org/10.1016/B978-0-444-63522-8.00015-2>.
- Villagran, X. 2019. "The Shell Midden Conundrum: Comparative Micromorphology of Shell-Matrix Sites From South America." *Journal of Archaeological Method and Theory* 26: 344–395. <https://doi.org/10.1007/s10816-018-9374-2>.
- Villagran, X. S., A. L. Balbo, M. Madella, A. Vila, and J. Estevez, 2011. "Stratigraphic and Spatial Variability in Shell Middens: Microfacies Identification at the Ethnohistoric Site Tunel VII (Tierra del Fuego, Argentina)." *Archaeological and Anthropological Sciences* 3: 26: 357–378. <https://doi.org/10.1007/s12520-011-0074-z>.
- Villagran, X., C. Flores, L. Olguín, et al. 2021. "Microstratigraphy and Faunal Records From a Shell Midden on the Hyperarid Coast of the Atacama Desert (Taltal, Chile)." In *South American Contributions to World Archaeology*, edited by M. Bonomo, S. Archila, 249–281. Springer Nature Switzerland AG. https://doi.org/10.1007/978-3-030-73998-0_10.
- Villagran, X., P. Giannini, and P. DeBlasis. 2009. "Archaeofacies Analysis: Using Depositional Attributes to Identify Anthropogenic Processes of Deposition in a Monumental Shell Mound of Santa Catarina State, Southern Brazil." *Geoarchaeology* 24: 311–335. <https://doi.org/10.1002/gea.20269>.
- Villagran, X., D. Huisman, S. Mentzer, C. Miller, and M. Jans. 2017. "Bone and Other Skeletal Tissues." In *Archaeological Soil and Sediment Micromorphology*, edited by C. Nicosia and G. Stoops, 9–38. Wiley Blackwell. <https://doi.org/10.1002/9781118941065.ch1>.
- Villagran, X., L. C. R. Pessenda, H. A. Valadares Costa, et al. 2018. "Os primeiros povoadores do litoral norte do Espírito Santo: Uma nova abordagem na arqueologia de sambaquis capixabas." *Boletim do Museu Paraense Emílio Goeldi. Ciências Humanas* 13: 573–596. <https://doi.org/10.1590/1981.81222018000300006>.
- Villagran, X., A. Strauss, C. Miller, B. Ligouis, and R. Oliveira. 2017. "Buried in Ashes: Site Formation Processes at Lapa do Santo Rock-shelter, East-Central Brazil." *Journal of Archaeological Science* 77: 10–34. <https://doi.org/10.1016/j.jas.2016.07.008>.
- Villagran, X. S. 2014. "A Redefinition of Waste: Deconstructing Shell and Fish Mound Formation Among Coastal Groups of Southern Brazil." *Journal of Anthropological Archaeology* 36: 211–227. <https://doi.org/10.1016/j.jaa.2014.10.002>.
- Ward, I., P. Moe-Astrup, and K. Merigot. 2019. "At the Water's Edge: Micromorphological and Quantitative Mineral Analysis of a Submerged Mesolithic Shell Midden at Hjørnø Sund, Denmark." *Journal of Archaeological Science* 102: 11–25. <https://doi.org/10.1016/j.jas.2018.12.009>.
- Weiner, S. 2010. *Microarchaeology*. Cambridge University Press.
- Weiner, S., P. Goldberg, and O. Bar-Yosef. 2002. "Three-Dimensional Distribution of Minerals in the Sediments of Hayonim Cave, Israel: Diagenetic Processes and Archaeological Implications." *Journal of Archaeological Science* 29: 1289–1308. <https://doi.org/10.1006/jasc.2001.0790>.

White, W. 1974. "The Carbonate Minerals." In *The Infrared Spectra of Minerals*, edited by V. C. Farmer, 227–284. Mineralogical Society of Great Britain and Ireland.

Widmer, R. J. 2014. "The Key Marco Site, a Planned Shell Mound Community on the Southwest Florida Coast." In *The Cultural Dynamics of Shell-Matrix Sites*, edited by M. Roksandic, S. Mendonça de Souza, S. Eggers, M. Burchell, and D. Klokler, 11–20. University of New Mexico Press.

Williams, A. J., M. Pagliai, and G. Stoops. 2018. "Physical and Biological Surface Crusts and Seals." In *Interpretation of Micromorphological Features of Soils and Regoliths*, edited by G. Stoops, V. Marcelino, and F. Mees, 539–574. Elsevier. <https://doi.org/10.1016/B978-0-444-63522-8.00019-X>.

Wurz, S., R. Pickering, and S. Mentzer. 2022. "U-Th Dating, Taphonomy, and Taxonomy of Shell Middens at Klasies River Main Site Indicate Stable and Systematic Coastal Exploitation by MIS 5C-D." *Frontiers in Earth Science* 10: 1–25. <https://doi.org/10.3389/feart.2022.1001370>.

Zenero, J. 2022. "Modelo preditivo arqueológico do alto vale do Ribeira de Iguape e resultados do sítio Paredão Consteca." Master's diss., University of São Paulo. <https://www.teses.usp.br/teses/disponiveis/71/71131/tde-29032023-145434/ptbr.php>.

Zerboni, A. 2011. "Micromorphology Reveals In Situ Mesolithic Living Floors and Archaeological Features in Multiphase Sites in Central Sudan." *Geoarchaeology* 26: 365–391. <https://doi.org/10.1002/gea.20355>.

Zhang, Y., F. Qin, X. Pu, W. Wei, and P. J. Piper. 2024. "Chronological Analysis of Prehistoric Freshwater Shell Mounds in the Yongjiang River Basin, Guangxi, China." *Archaeological Research in Asia* 37: 100502. <https://doi.org/10.1016/j.ara.2024.100502>.

Supporting Information

Additional supporting information can be found online in the Supporting Information section.